Analysis and Modeling of the Arctic Oscillation Using a Simple Barotropic Model with Baroclinic Eddy Forcing

H. L. TANAKA

Frontier Research System for Global Change, International Arctic Research Center, University of Alaska Fairbanks, Fairbanks, Alaska, and Institute of Geoscience, University of Tsukuba, Tsukuba, Japan

(Manuscript received 8 March 2002, in final form 19 December 2002)

ABSTRACT

In this study, a numerical simulation of the Arctic Oscillation (AO) is conducted using a simple barotropic model that considers the barotropic–baroclinic interactions as the external forcing. The model is referred to as a barotropic S model since the external forcing is obtained statistically from the long-term historical data, solving an inverse problem. The barotropic S model has been integrated for 51 years under a perpetual January condition and the dominant empirical orthogonal function (EOF) modes in the model have been analyzed. The results are compared with the EOF analysis of the barotropic component of the real atmosphere based on the daily NCEP–NCAR reanalysis for 50 yr from 1950 to 1999.

According to the result, the first EOF of the model atmosphere appears to be the AO similar to the observation. The annular structure of the AO and the two centers of action at Pacific and Atlantic are simulated nicely by the barotropic S model. Therefore, the atmospheric low-frequency variabilities have been captured satisfactorily even by the simple barotropic model.

The EOF analysis is further conducted to the external forcing of the barotropic S model. The structure of the dominant forcing shows the characteristics of synoptic-scale disturbances of zonal wavenumber 6 along the Pacific storm track. The forcing is induced by the barotropic–baroclinic interactions associated with baroclinic instability.

The result suggests that the AO can be understood as the natural variability of the barotropic component of the atmosphere induced by the inherent barotropic dynamics, which is forced by the barotropic–baroclinic interactions. The fluctuating upscale energy cascade from planetary waves and synoptic disturbances to the zonal motion plays the key role for the excitation of the AO.

1. Introduction

The Arctic Oscillation (AO) postulated by Thompson and Wallace (1998, 2000) has attracted more attention in recent years. The AO is a north–south seesaw of the atmospheric mass between the Arctic region poleward of 60°N and a surrounding zonal ring in the midlatitudes. It is defined as a primary mode of an empirical orthogonal function (EOF) for the sea level pressure field in the Northern Hemisphere. The spatial pattern of the AO is characterized by its zonally symmetric or "annular" structure centered in the Arctic. The AO bears a superficial resemblance to the leading mode of low-frequency variability in the Southern Hemisphere, which is now referred to as a Southern Hemisphere annular mode (SAM). In this regard, a terminology of Northern Hemisphere annular mode (NAM) is preferred for the AO by Wallace (2000). In this study, we will refer to the AO as the EOF-1 of atmospheric variability with one sign over the Arctic and two poles of opposite sign over the Pacific and Atlantic sectors, while the terminology of the annular mode is reserved essentially for the zonally symmetric variation in the atmosphere.

The AO is successfully simulated by a number of realistic general circulation models with fixed forcing (Feldstein and Lee 1998; Yamazaki and Shinya 1999; Fyfe et al. 1999; Shindell et al. 1999; Limpasuvan and Hartmann 1999, 2000; Boer et al. 2001; Robertson 2001). The basic features of the zonally symmetric structures are also simulated using simple quasigeostrophic and primitive equation models with simple physics and no topography or seasonal cycle (Robinson 1991, 1994, 1996; James and James 1992; Yu and Hartmann 1993; Lee and Feldstein 1996; Feldstein and Lee 1998; Akahori and Yoden 1997). Because the external forcing of the model is independent of time, the variability found in these simple models is the unforced variability associated with dynamical processes internal to the atmosphere (Feldstein 2002). The dynamical examination of the annular modes shows that the baroclinic eddies in midlatitudes played an important role for the internal variability of the zonal mean flow through the positive feedback in momentum budget between the eddies and the mean flow (Karoly 1990; Shiotani

Corresponding author address: Dr. H. L. Tanaka, Insitute of Geoscience, University of Tsukuba, Tsukuba 305-8571, Japan.
E-mail: tanaka@atm.geo.tsukuba.ac.jp

1990; Hartmann 1995; Kidson and Sinclair 1995; Hartmann and Lo 1998; Yamazaki and Shinya 1999; Lorenz and Hartmann 2001; Tanaka and Tokinaga 2002).

Shiotani (1990) showed that the vacillation between the eddies and the mean flow is the essential mechanism for the SAM. Yamazaki and Shinya (1999) analyzed the Eliassen–Palm (EP) flux divergence and found that the wave–mean flow interactions by planetary waves provide the largest contribution to the positive feedback while the synoptic-scale waves contribute destructively to the NAM. Lorenz and Hartmann (2001) analyzed the zonal-mean zonal wind anomaly in the Southern Hemisphere and showed that an equivalent barotropic dipole with opposite anomalies at 40° and 60°S indicates a positive feedback with low-frequency eddy forcing to maintain the persistent anomaly associated with the SAM. A similar conclusion was attained by Tanaka and Tokinaga (2002), who analyzed baroclinic instability associated with the polar jet. While the ordinary Charney mode excited by the subtropical jet brings eddy momentum southward in high latitudes to intensify the subtropical jet, the baroclinic instability excited by the polar jet brings the eddy momentum northward to intensify the polar jet. Since the polar baroclinic mode tends to dominate when the polar jet is strong, the positive feedback plays an essential role in maintaining the anomaly of the polar jet, which may in turn result in the NAM.

Despite the argument with simple general circulation models, the dynamical interpretation of the AO is still an open question. An attempt to understand the essential part of the dynamics of the AO may be desired with further simplified models. According to the observational analysis, the AO has an equivalent barotropic structure from the surface to the lower stratosphere in that the positive or negative geopotential anomaly occurs consistently from the troposphere to the stratosphere (Kodera et al. 1996; Kitoh et al. 1996; Thompson and Wallace 1998). Based on this fact, even a simple barotropic model may be used to simulate a robust structure of the AO.

The purpose of this study is to demonstrate that the realistic AO can be simulated by a simple barotropic model with a suitable external forcing representing the barotropic–baroclinic interactions. Such a barotropic model has been constructed in our previous studies from a 3D spectral primitive equation model using only the component of the vertical wavenumber zero of the model. According to the observational analysis, the barotropic–baroclinic interactions are achieved mostly by synoptic disturbances (Tanaka 1985; Tanaka and Kung 1988). With the knowledge of the linear solutions of baroclinic instability on a sphere (Tanaka and Kung 1989; Tanaka and Sun 1990), the barotropic–baroclinic interactions have been parameterized by Tanaka (1991, 1998) to close the barotropic model. With the parameterized baroclinic instability as the main energy source, the barotropic model was integrated to simulate realistic blocking (Tanaka 1991, 1998). Recently, the model has been applied to the actual forecasting of the barotropic component of the atmosphere (Tanaka and Nohara 2001). We demonstrated that the model has a meaningful deterministic predictability of 8 days, which is comparable to the operational weather forecasting models. In this study the model was integrated for 51 yr under a perpetual January condition to simulate the realistic pattern of the AO. The result of the EOF analysis of the model atmosphere was compared with the observed EOF patterns using the National Centers for Environmental Prediction (NCEP) and National Center for Atmospheric Research (NCAR) reanalysis for 50 yr from 1950 to 1999 (see Kalnay et al. 1996).

In section 2 the governing equations and the data used in this study are described. In section 3 the result of the EOF analysis is presented for the observed atmosphere in order to compare with that of the model atmosphere. The results of the 51-yr time integration of the model and the dominant EOF modes are presented in section 4. Finally, in section 5, the dynamical interpretation of the AO is discussed in reference to the energetics analysis of the AO.

2. Method and data

a. Governing equations

The model description is provided by Tanaka (1998) and Tanaka and Nohara (2001), so a brief description is presented here. A system of primitive equations with a spherical coordinate of longitude λ, latitude θ, pressure p, and time t may be reduced to three prognostic equations of horizontal motions and thermodynamics for three dependent variables of $\mathbf{U} = (u, v, \phi')^{\mathrm{T}}$. Here, u and v are the zonal and meridional components of the horizontal velocity, respectively, and ϕ' is a departure of the local isobaric geopotential from the reference state geopotential ϕ_0. The superscript "T" denotes a transpose. Using a matrix notation, these primitive equations may be written as

$$\mathbf{M}\frac{\partial \mathbf{U}}{\partial t} + \mathbf{L}\mathbf{U} = \mathbf{N} + \mathbf{F}, \tag{1}$$

where the left-hand side of (1) represents linear terms with matrix operators $\mathbf{M}$ and $\mathbf{L}$ and the dependent variable vector $\mathbf{U}$. Refer to Tanaka (1998) for the definition of matrices $\mathbf{M}$ and $\mathbf{L}$. The right-hand side represents a nonlinear term vector $\mathbf{N}$ and a diabatic term vector $\mathbf{F}$, which includes the zonal and meridional components of frictional forces and a diabatic heating rate.

In order to obtain a system of 3D spectral primitive equations, we expand the vectors $\mathbf{U}$ and $\mathbf{F}$ in 3D normal mode functions in a resting atmosphere, $\Pi_{nlm}(\lambda, \theta, p)$:

$$\mathbf{U}(\lambda, \theta, p, t) = \sum_{nlm} w_{nlm}(t) X_m \Pi_{nlm}(\lambda, \theta, p), \tag{2}$$

$$\mathbf{F}(\lambda, \theta, p, t) = \sum_{nlm} f_{nlm}(t) Y_m \Pi_{nlm}(\lambda, \theta, p), \tag{3}$$

where the dimensionless expansion coefficients $w_{nlm}(t)$ and $f_{nlm}(t)$ are the functions of time alone. These may be computed by the inverse Fourier transforms of **U** and **F** from the observed data.

$$w_{nlm}(t) = \langle \mathbf{U}(\lambda, \theta, p, t), \mathbf{X}_m^{-1}\Pi_{nlm}(\lambda, \theta, p)\rangle, \quad (4)$$

$$f_{nlm}(t) = \langle \mathbf{F}(\lambda, \theta, p, t), \mathbf{Y}_m^{-1}\Pi_{nlm}(\lambda, \theta, p)\rangle. \quad (5)$$

The subscripts represent zonal wavenumbers n, meridional indices l, and vertical indices m. The scaling matrices $\mathbf{X}_m$ and $\mathbf{Y}_m$ are defined at each vertical index. The expansion basis of the 3D normal mode functions $\Pi_{nlm}(\lambda, \theta, p)$ is obtained as an eigensolution of a homogeneous partial differential equation, putting zero on the right-hand side of (1). The 3D normal mode functions are given by a tensor product of vertical structure functions $G_m(p)$ and Hough harmonics $H_{nlm}(\lambda, \theta)$ associated with the linear operators **M** and **L**, respectively (Kasahara 1976, 1978). They form a complete set and satisfy an orthonormality condition under a proper inner product $\langle\ ,\ \rangle$.

By expanding those variables in 3D normal mode functions, we obtain a system of 3D spectral primitive equations in terms of the spectral expansion coefficients:

$$\frac{dw_i}{d\tau} + i\sigma_i w_i = -i \sum_{jk} r_{ijk} w_j w_k + f_i, \quad i = 1, 2, 3, \ldots, \quad (6)$$

where τ is a dimensionless time scaled by $(2\Omega)^{-1}$, Ω is the angular speed of the earth's rotation, σ_i is the eigenfrequency of the Laplace's tidal equation, and r_{ijk} is the interaction coefficients for nonlinear wave–wave interactions calculated by the triple products of the 3D normal mode functions. The triple subscripts are shortened for simplicity as $w_{nlm} = w_i$. There should be no confusion in the use of i for a subscript even though it is used for the imaginary unit in (6).

b. Construction of a barotropic S model

In the 3D spectral representation, the vertical expansion basis functions may be divided into barotropic ($m = 0$) and baroclinic ($m \neq 0$) components. We may construct a simple spectral barotropic model, using only the barotropic components ($m = 0$) of the Rossby modes, by truncating all the baroclinic modes and high-frequency gravity modes (see Kasahara 1977). Such a model is equivalent to a model predicting the vertical average of meteorological variables. The barotropic components capture the essential features of the low-frequency variability of planetary-scale motions. The spectral equation for such a barotropic model may be written as

$$\frac{dw_i}{d\tau} + i\sigma_i w_i = -i \sum_{jk} r_{ijk} w_j w_k + f_i + g_i, \quad i = 1, 2, 3, \ldots, \quad (m = 0), \quad (7)$$

where the indices of the subscripts run only for the barotropic modes. The zonal and meridional wave truncation of the present model is equivalent to rhomboidal 20 with an equatorial wall. The degree of freedom of the system is reduced enormously by these truncations. The spectral equation for such a barotropic model (7) has the same form as for the baroclinic model equation (6), except for the fact that the barotropic–baroclinic interaction g_i appears on the right-hand side. Henceforth, we combine $f_i + g_i$ and designate it as the external forcing s_i of the barotropic model.

The parameterization of the external forcing $s_i = f_i + g_i$ in (7) is presented by Tanaka (1991, 1998) considering the dynamical processes of the baroclinic instability, the topographic forcing, the biharmonic diffusion, the zonal surface stress, and the Ekman pumping. Since those parameterizations are fundamentally linear approximations to the true forcing and will never be a perfect representation of the real atmosphere, we have attempted in this study to obtain the best linear fit of the forcing s_i based on the 50 yr of the NCEP–NCAR reanalysis from 1950 to 1999 as in Tanaka and Nohara (2001):

$$s_i = \tilde{s}_i + s_i' = \tilde{s}_i + \mathbf{A}_{ij} w_j + \mathbf{B}_{ij} w_j^* + \epsilon_i, \quad (8)$$

where $\tilde{s}_i$ and s_i' are the climate and anomaly of s_i, respectively. The asterisk for w_i represents a complex conjugate of w_i. In general, w_i and w_i^* are linearly independent, and both are required in the complex-valued regression since only the positive (and zero) zonal wavenumbers are considered for the state variables of the model. We can evaluate the perfect external forcing of s_i from the observation as the residual of Eq. (7). The climate $\tilde{s}_i$ is obtained by the time mean of s_i for the 50-yr period. The first four harmonics of the seasonal change are synthesized to get a smooth seasonal march of $\tilde{s}_i$, and the anomaly s_i' is evaluated as the deviation from it.

The unknown linear matrices $\mathbf{A}_{ij}$ and $\mathbf{B}_{ij}$ can be obtained by the standard method of the least square fitting for s_i' to minimize the regression residual. In the stepwise least square fitting method, the matrix $\mathbf{A}_{ij}$ is evaluated first by

$$\mathbf{A}_{ij} = \overline{s_i' w_j^+}, \quad (9)$$

where, $s_i' = s_i - \tilde{s}_i$, $\overline{(\ )}$ is the time mean, and w_j^+ is referred to as the pseudoinverse of w_j defined by

$$w_j^+ = w_k^H \overline{(w_k w_j^H)}^{-1}, \quad (10)$$

where the superscript H denotes a complex conjugate transpose. It is a linear inverse problem (see Winkler et al. 2001) to obtain the system matrix from the known data of w_i and s_i'. Similarly, the matrix $\mathbf{B}_{ij}$ may be obtained by minimizing the remainder ϵ_i by regressing the first residual δ_i, which is obtained by the first regression associated with $\mathbf{A}_{ij}$:

$$\mathbf{B}_{ij} = \overline{\delta_i w_j^{*+}}, \quad (11)$$

using the pseudoinverse of w_j^*.

The model with such a forcing is named "barotropic

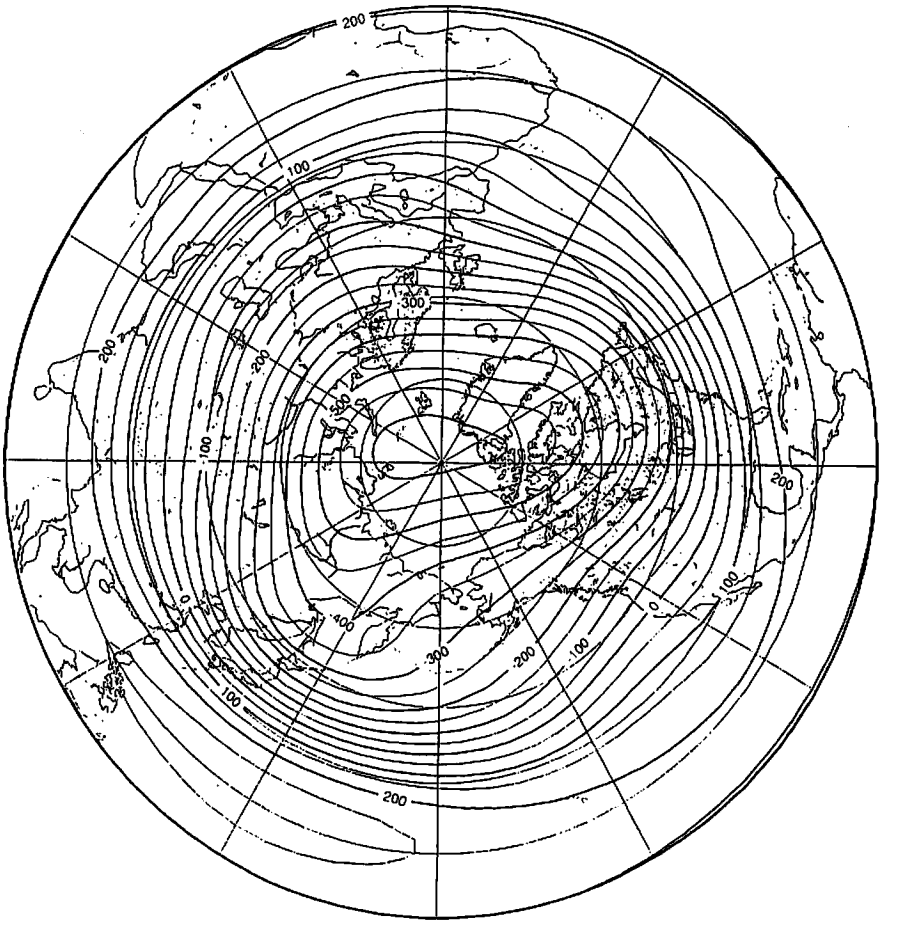

FIG. 1. Mean barotropic height (in m) averaged for the winter mean (DJF) with the NCEP–NCAR reanalysis from 1950 to 1999.

S model" since the forcing is obtained statistically from observation, solving the inverse problem. The application of the barotropic S model to real forecasting is demonstrated by Tanaka and Nohara (2001), showing the mean predictability of 8 days according to the anomaly correlation. Although the barotropic S model demonstrates considerable predictability, the synoptic eddies appear to be weak by this formulation. The system matrices $\mathbf{A}_{ij}$ and $\mathbf{B}_{ij}$ mostly represent topographic forcing (TF). For this reason, we have added the energy source in terms of the parameterized baroclinic instability (BC) described by Tanaka (1998). The increased energy source at the synoptic scale requires an additional energy sink, so the biharmonic diffusion (DF), the zonal surface stress (DZ), and the Ekman pumping (DE) are also included in reference to the resulting energy spectrum of the model climate. The final form of the external forcing s_i is expressed as

$$s_i = \tilde{s}_i + \mathbf{A}_{ij}w_j + \mathbf{B}_{ij}w_j^* + (\mathrm{BC})_{ij}w_j + (\mathrm{DF})_{ij}w_j + (\mathrm{DZ})_{ij}w_j + (\mathrm{DE})_{ij}w_j. \quad (12)$$

Note that the topographic forcing is contained in $\tilde{s}_i$, as well as the system matrices. Although the barotropic–baroclinic interaction is implicitly considered in the model, the forcing has been modeled entirely by the barotropic component of the state variables w_i. Hence, any variability generated within the model may be considered as a natural variability governed by the barotropic dynamics internal to the model atmosphere.

c. Data and procedures

The data used in this study are four-times-daily NCEP–NCAR reanalysis for 51 yr from 1950 to 2000 (see Kalnay et al. 1996). The data contain horizontal winds $V = (u, v)$ and geopotential ϕ, defined at every 2.5° latitude by 2.5° longitude grid point over 17 mandatory vertical levels from 1000 to 10 hPa.

The expansion coefficients w_i are obtained by the inverse Fourier transform of (4) from the dataset of $\mathbf{U} = (u, v, \phi')$. Although the data are recorded 4 times

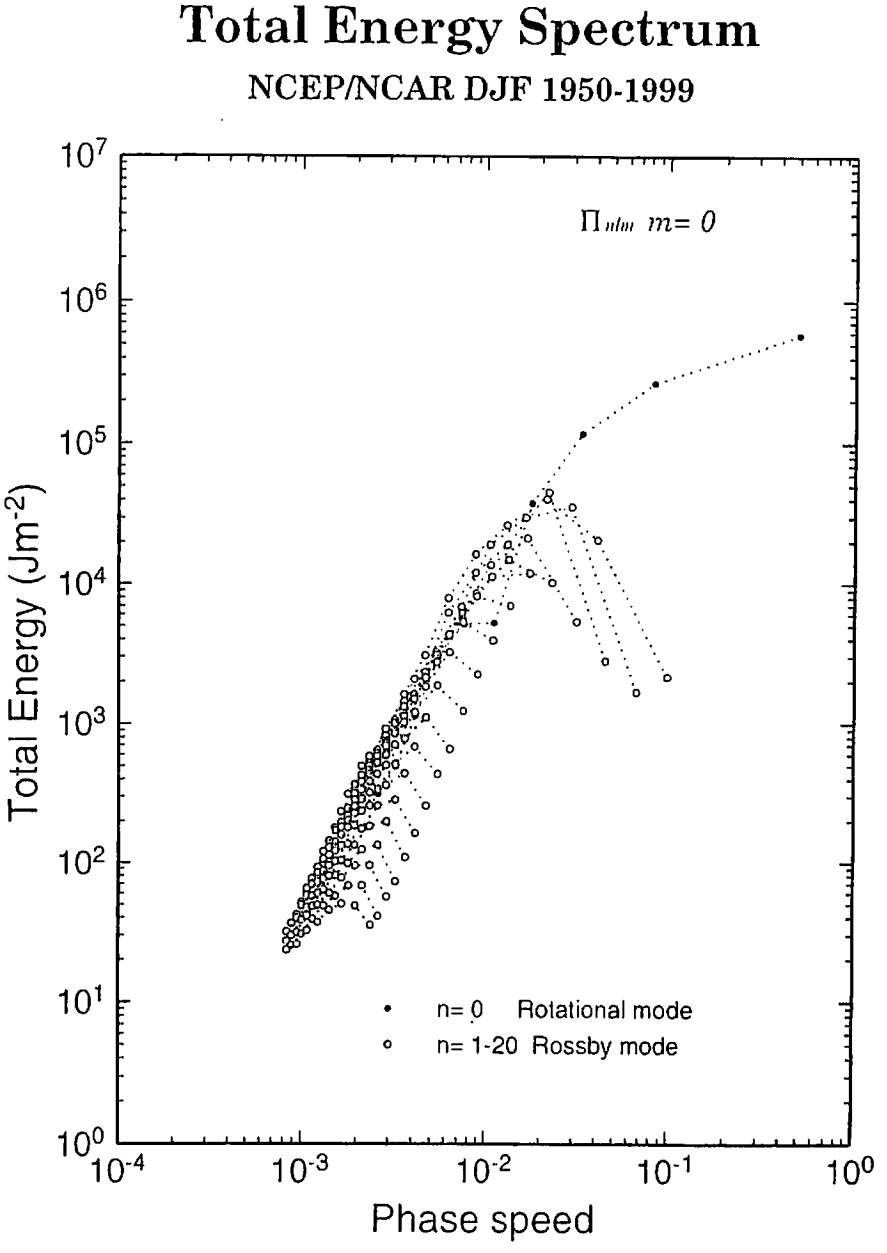

FIG. 2. Barotropic energy spectrum of E_{nlm} as a function of the dimensionless scale index $|c_{nlm}|$ evaluated for the 50 yr of the NCEP–NCAR reanalysis during winter. The black and white dots denote $n = 0$ and $n \neq 0$, respectively. (Unit: J m^{-2}.)

daily, we refer to it as daily data in subsequent sections since the diurnal variation of w_i is removed by a time filter. The external forcing $s_i = f_i + g_i$ is then diagnostically calculated by (7) as the residual of the equation, which provides the climate $\bar{s}_i$ and the anomaly s_i' in (8). The EOF analysis is applied to the time series of w_i and s_i for the 50-yr data from 1950 to 1999 to find the dominant mode in the real atmosphere. With the known w_i and s_i, the linear matrices $\mathbf{A}_{ij}$ and $\mathbf{B}_{ij}$ in (8) are computed by (9) and (11) based on the data for December–January–February (DJF) during the 50 yr. The year 2000 is reserved for a statistically independent forecasting as demonstrated by Tanaka and Nohara (2001). Finally, the barotropic S model of (7) is integrated for 51 yr under a perpetual January condition, starting from the initial data of w_i at 0000 UTC on 1 January 1950 with the value of $\bar{s}_i$ fixed on 1 January.

3. Dominant modes of the observed atmosphere

a. Barotropic component of the atmosphere

In general, the low-frequency variabilities such as AO, North Atlantic Oscillation (NAO), and Pacific–North America (PNA) are characterized by the equivalent barotropic structure. In this study, the 3D structures of atmospheric variables are projected onto the barotropic component of the vertical normal mode functions:

$$(u,\ v,\ \phi')_0^{\mathrm{T}} = \frac{1}{p_s}\int_0^{p_s} (u,\ v,\ \phi')^{\mathrm{T}} G_0\, dp. \qquad (13)$$

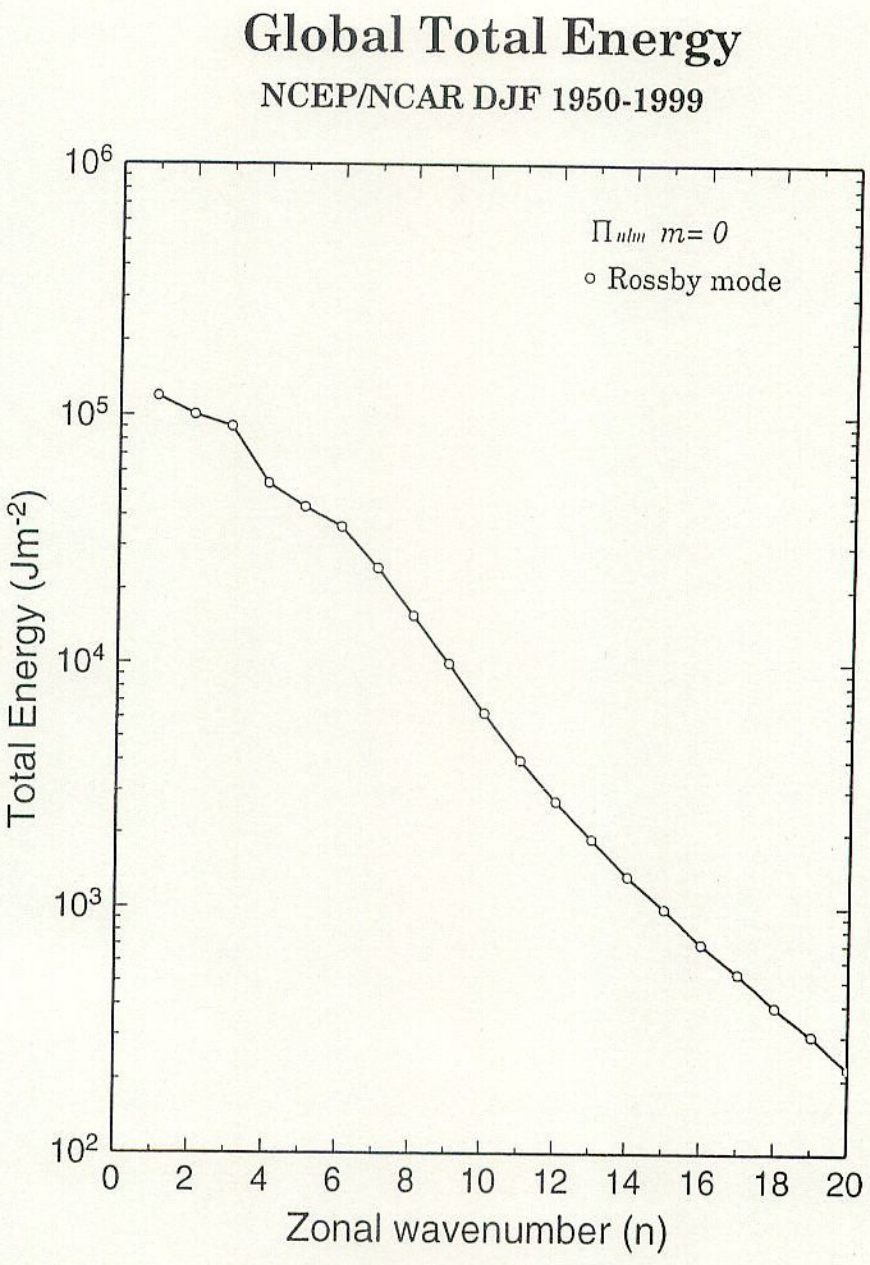

FIG. 3. Barotropic energy spectrum as a function of the zonal wavenumber n by summing all meridional indices in Fig. 2. (Unit: J m^{-2}.)

Here, G_0 is the vertical normal mode of $m = 0$, and p_s is the surface pressure of the reference state. It is a part of the inverse Fourier transform of (4) associated with the vertical transform. The vertical transform (13) is followed by the Fourier–Hough transforms to obtain the expansion coefficient w_i in (4). Since the structure of G_0 is approximately constant with no node in the vertical, the vertical transform for $m = 0$ may be regarded as the vertical mean of the state variables. In this study, the left-hand side of (13) is referred to as a barotropic component of the atmosphere that depends only on longitude, latitude, and time.

Figure 1 illustrates the barotropic component of the geopotential height averaged for the winter (DJF) from 1950 to 1999. In order to obtain this figure, the expansion coefficients w_i are averaged for 50 yr in the spectral domain, then the mean w_i is converted to the geopotential field using Eq. (2). Since geopotential height is defined by the deviation from the global mean as discussed in (1), the value is negative at the polar region and is positive in the Tropics. We will refer to it as a barotropic height.

In the spectral domain, total energy E (sum of kinetic energy and available potential energy) is simply the sum of the energy elements E_i defined by

$$E_i = \frac{1}{2} p_s h_m |w_i|^2, \tag{14}$$

where h_m is the equivalent depth of the vertical mode m. The 3D scale of the normal mode has been defined in Tanaka (1985) by the eigenfrequency of Laplace's tidal equation σ_i in (6). Especially for the Rossby mode, the suitable choice of the scale index is the westward

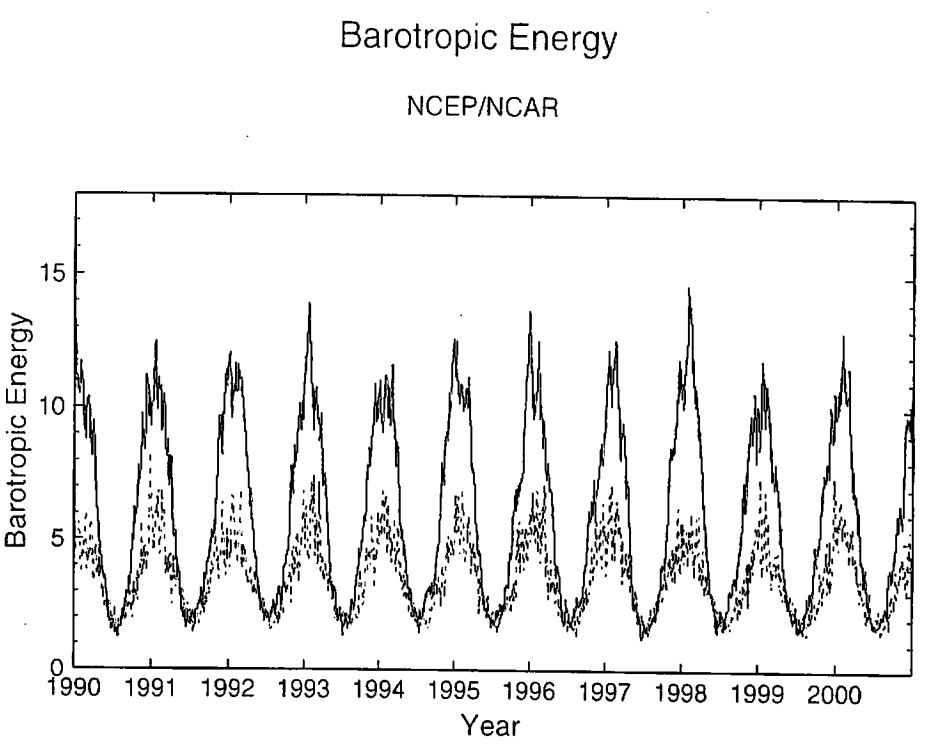

FIG. 4. Daily time series of barotropic energy from 1990 to 2000. The solid and dashed lines represent zonal ($n = 0$) and eddy ($n \neq 0$) energy, respectively. (Unit: 10^5 J m^{-2}.)

phase speed $c_i = \sigma_i/n$. It is known from the Rossby wave dispersion that the larger the Rossby mode is, the larger the westward phase speed is. (There is an exception in planetary waves for the Hough modes.) Therefore, the westward phase speed $|c_i|$ represents the 3D scale of the Rossby mode. The energy spectrum of E_i as a function of the scale index $|c_i|$ was analyzed by Tanaka and Kasahara (1992), showing that the spectrum over the scale index $|c_i|$ obeys a unique power law even for the zonal wavenumber zero. For zonal wavenumber zero, the scale index is not defined because Laplace's tidal equation degenerates for Rossby modes. All eigenvalues of σ_i are zero for $n = 0$. The difficulty was overcome by the use of Shigehisa modes (Shigehisa 1983) where mathematical limits of $c_i = \sigma_i/n$ converge to finite values. The energy spectrum for $n = 0$ over $|c_i|$ appears to coincide with that of $n \neq 0$ for the small meridional scale. It was demonstrated in Tanaka (1991) that the phase speed of the geostrophic mode proposed by Kasahara (1978), which is used in this study, can be approximated by that of the Haurwitz wave on a sphere:

$$c_i = \frac{\sigma_i}{n} \approx \frac{-1}{l(l+1)}, \tag{15}$$

where l is the meridional mode number of $n = 0$. Using this definition of the scale index $|c_i|$ for $n = 0$, we can analyze the energy spectrum for all zonal waves, including $n = 0$.

Figure 2 plots the barotropic ($m = 0$) energy spectrum of $E_i = E_{nlm}$ as a function of the scale index $|c_i| = |c_{nlm}|$ evaluated for the 50 yr of the NCEP–NCAR reanalysis during winter. The dotted lines connect spectra for the same zonal wavenumber n over different meridional mode numbers l. The spectrum obeys approximately the third power of $|c_i|$, except for the largest-scale meridional modes, which indicate less energy levels. The peak of the energy spectrum for the zonal eddy $n \neq 0$ is basically determined by the Rhines' scale, where the inverse energy cascade from short waves to planetary waves terminates (Rhines 1979). It is interesting to note that the spectrum for $n = 0$ coincides with that of $n \neq 0$ for a smaller $|c_i|$, and it continues to increase as the meridional index l decreases. We can confirm that the scale index for $n = 0$ in (15) is a good approximation to the energy spectrum of the Shigehisa mode presented in Tanaka and Kasahara (1992).

Figure 3 plots the zonal energy spectrum for the barotropic component of the atmosphere as a function of the zonal wavenumber n by summing all meridional indices in Fig. 2. The energy level is 1.3×10^5 J m^{-2} for $n = 1$. It drops to 2.4×10^2 J m^{-2} for $n = 20$. The zonal energy is 10.6×10^5 J m^{-2} (not shown). The energy spectrum is used as a reference when the barotropic S model is constructed.

Figure 4 plots the daily time series of total energy for the barotropic component of the atmosphere from 1990 to 2000. The solid and dashed lines represent zonal and eddy energy, respectively. The time series is simply the sum of E_i for zonal wavenumber $n = 0$ and for $n \neq 0$ evaluated in the spectral domain. According to the result, barotropic zonal energy exceeds 10×10^5 J m^{-2} in winter, and eddy energy is about one-half of it. Barotropic energy is reduced to 2×10^5 J m^{-2} in summer. There are substantial interseasonal and interannual variability in E_i, and thus in w_i.

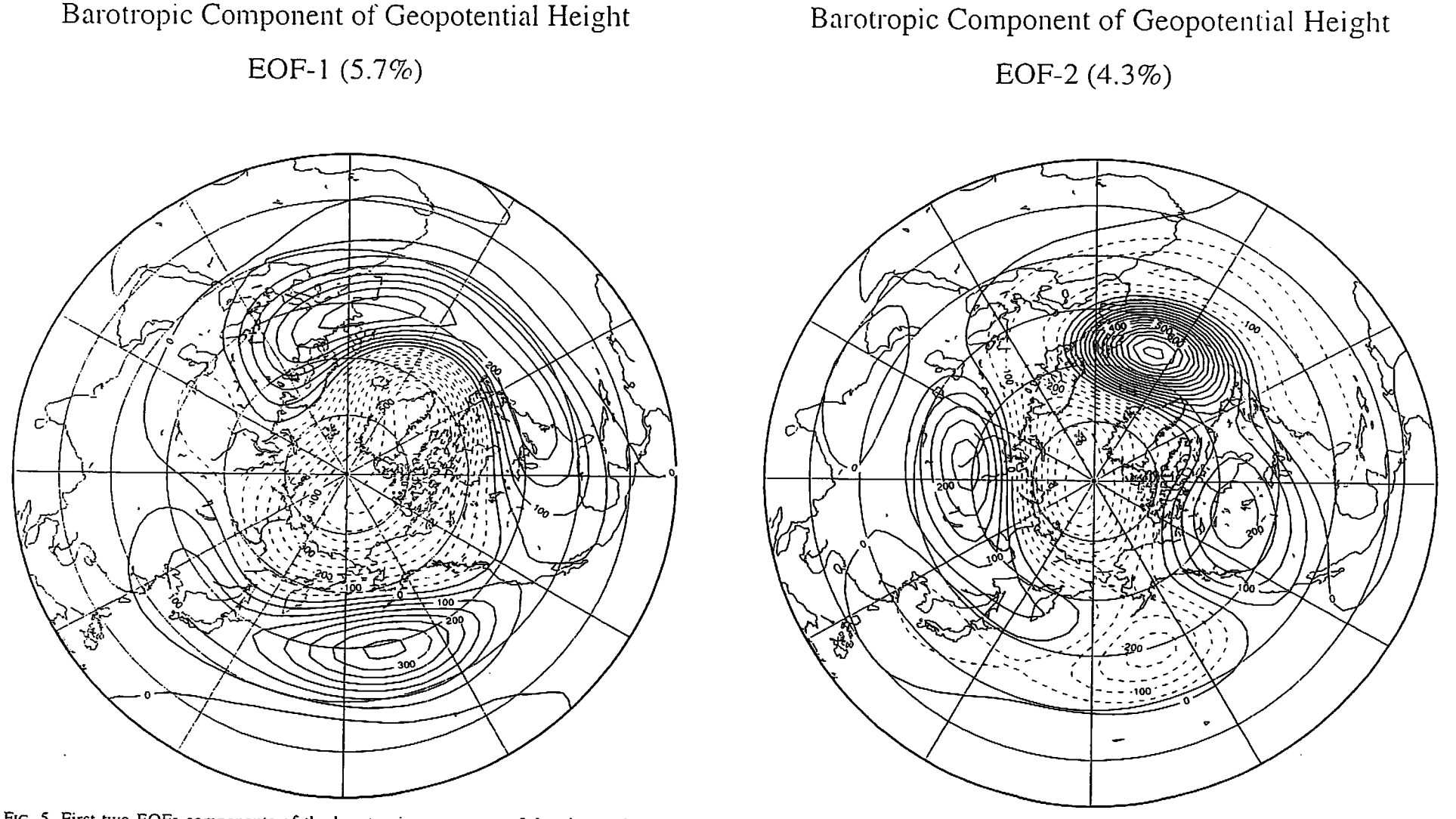

FIG. 5. First two EOFs components of the barotropic component of the observed atmosphere, analyzed by the state variable w_i with the daily NCEP–NCAR reanalysis from 1950 to 1999.

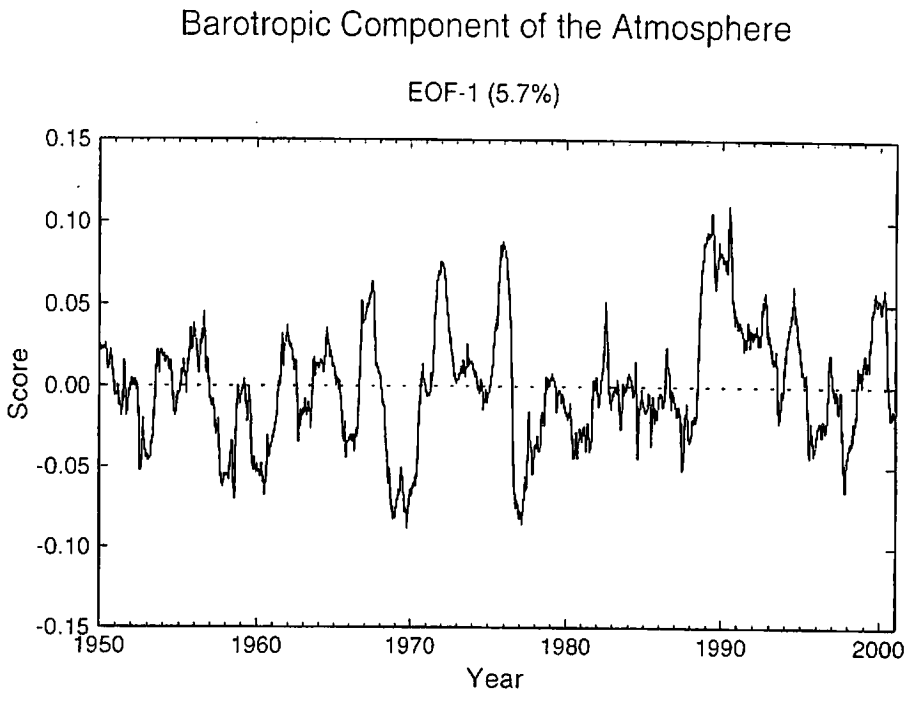

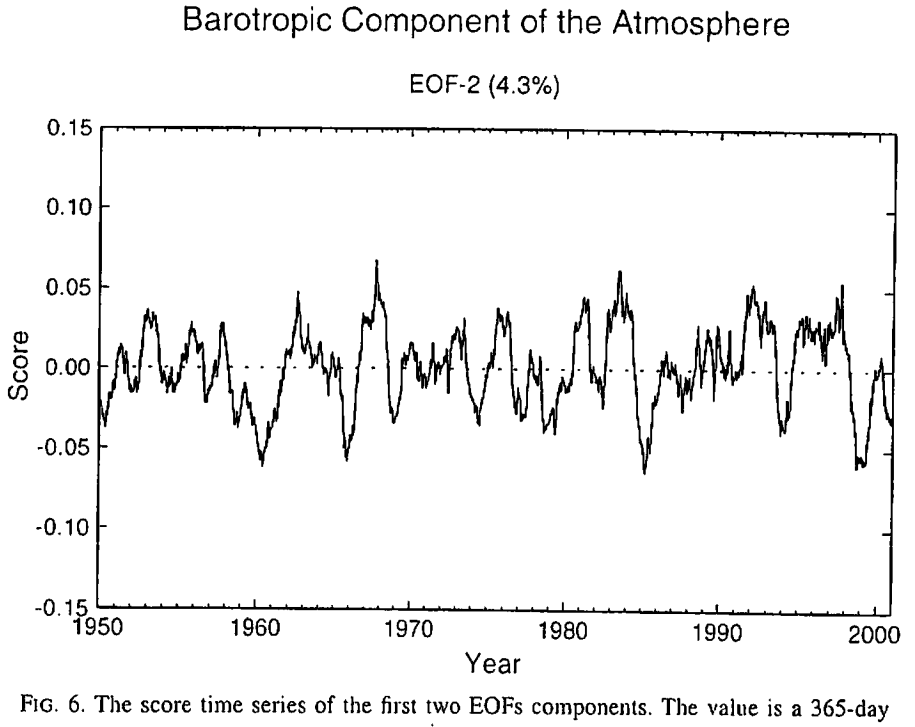

FIG. 6. The score time series of the first two EOFs components. The value is a 365-day running mean.

b. EOF analysis of the observed atmosphere

The climate of w_i with its seasonal march is computed from 50 yr of the time series data. Only the first four harmonics of the seasonal change are retained to get the smooth seasonal change of the climate of w_i. Once the climate is constructed, the anomaly of w_i is computed for the analysis period. The EOF analysis is then conducted for the anomaly time series of w_i in the spectral domain based on the daily data. The complex numbers of w_i are split in real and imaginary parts to compute the covariance matrix for the EOF analysis.

Figure 5 illustrates the first two EOF components of the atmosphere represented by the barotropic height. The structure of EOF-1 indicates a negative region in high latitudes surrounded by a positive region in the midlatitudes. The positive region shows two peaks over the Pacific and Atlantic sectors. The zero crossing is located around 60°N. The structure compares quite well with the AO analyzed by Thomp-

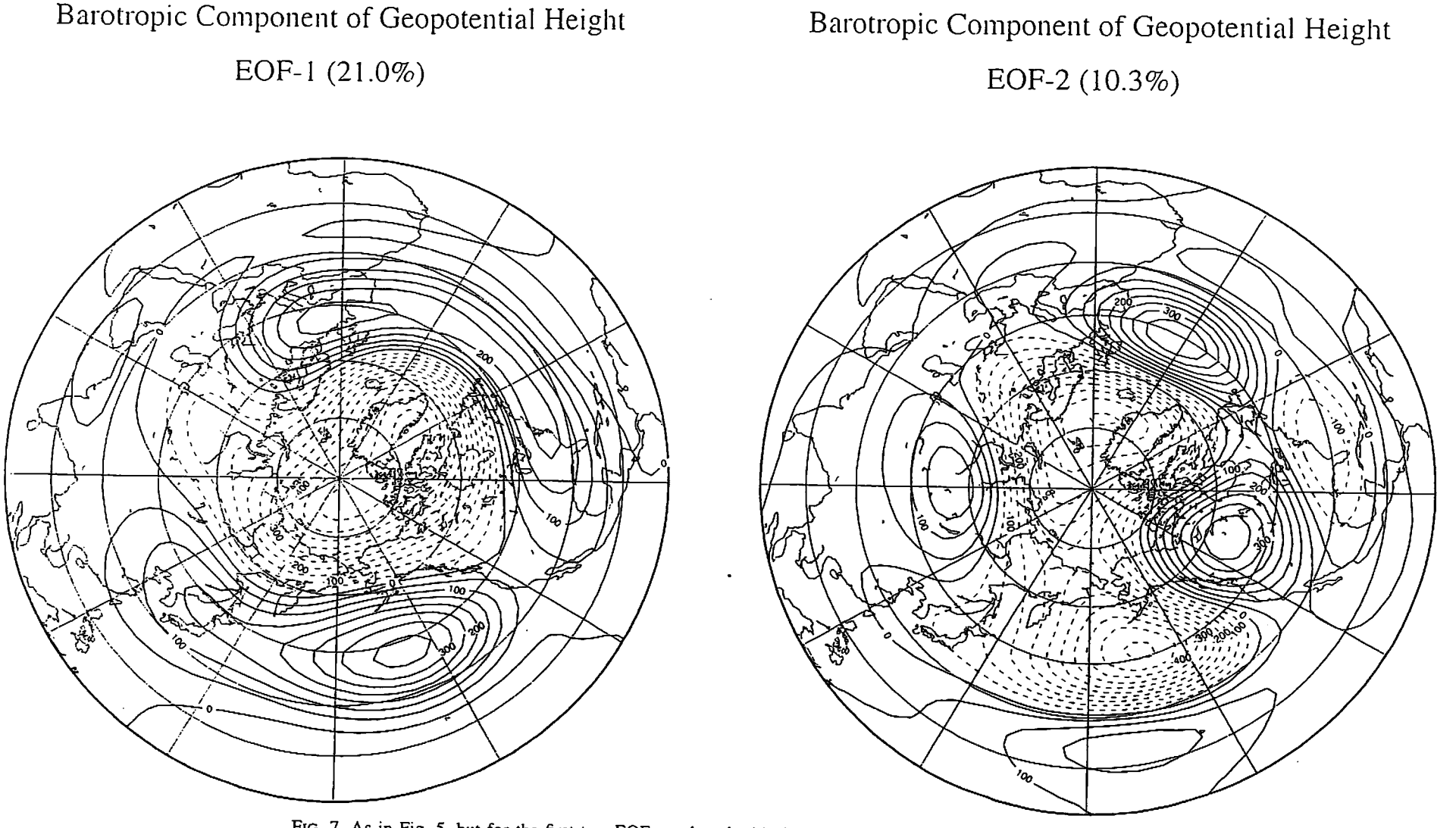

FIG. 7. As in Fig. 5, but for the first two EOFs analyzed with the winter mean (DJF) data from 1950 to 1999.

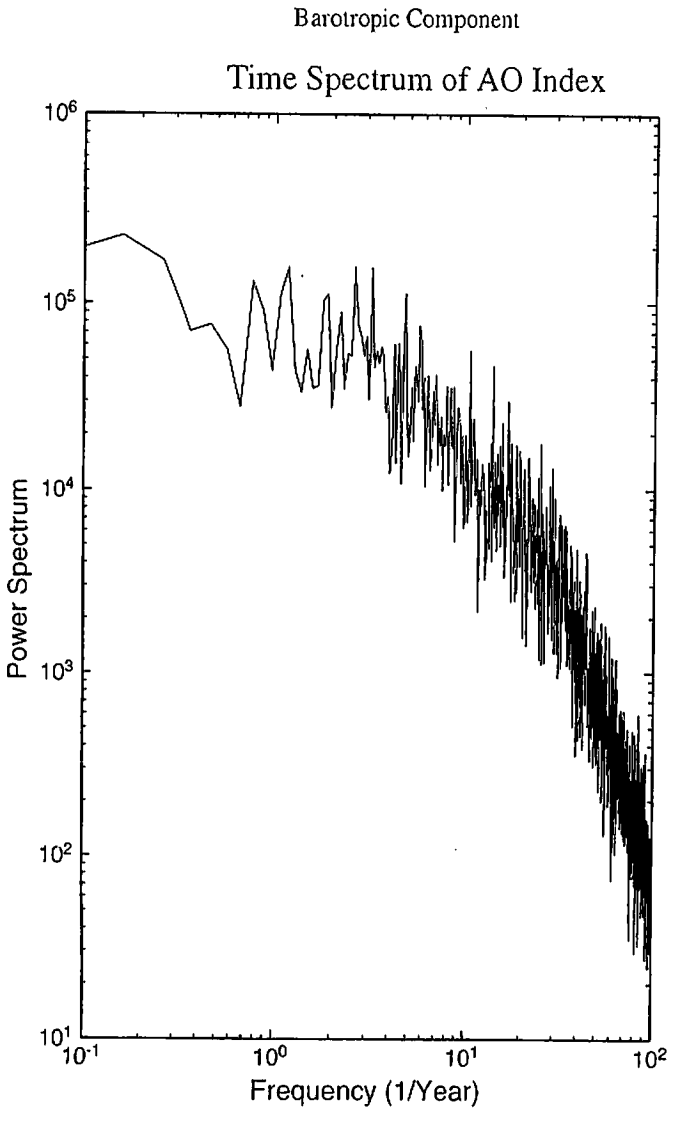

FIG. 8. The time spectrum of the daily AO index of EOF-1 in Fig. 6.

son and Wallace (1998), so EOF-1 of this study is easily identified as the AO. The original definition of the AO is based on sea level pressure, which is a single variable at a single level. It should be noted that our result is based on the whole column of vertical data using all state variables (u, v, ϕ) during 50 yr of the daily data. Although our EOF analysis is performed for the barotropic component from the beginning, EOF-1 should be recognized as the most dominant low-frequency variability in the 3D atmosphere since most of the low-frequency variabilities are contained in the barotropic component. Since the daily data contain active synoptic-scale eddies, it may be worth noting that the AO remains the most dominant mode even for the analysis with the daily data.

EOF-1 explains 5.7% of the total variance of the daily data. The score time series (365-day running mean) of the EOFs are plotted in Fig. 6. The time series of EOF-1 is referred to as the AO index, which represents considerable interannual variabilities. The positive value corresponds to a strong polar vortex while the negative value indicates a weak polar vortex. The AO index fluctuates between positive and negative values for 1950 to 1970, and it remains negative from 1976 to 1989. A notable shift from negative to positive occurs in 1989. The positive AO index then gradually decreases to a negative AO in the late 1990s, but it returns to positive in 2000. Clear decadal variability is contained in the AO index, but no significant trend is detected for the barotropic component of the atmosphere. According to the original definition of the AO index by Thompson and Wallace (1998), the decadal variability is superimposed on a recent trend related to global warming. Such a trend may be characterized in the baroclinic component of the atmosphere.

EOF-2 explains 4.3% of the total variance of the daily data. A negative area over the Arctic is surrounded by positive values in the midlatitudes, with three peaks over the Atlantic Ocean, Siberia, and Canada. The structure is similar to the AO, except for the opposite sign over the Atlantic and the Pacific sectors. The score time series of EOF-2 indicates interannual variability with a 2–3-yr period. The apparent decadal variability seen for EOF-1 is not obvious for EOF-2.

Figure 7 illustrates the result of the same EOF analysis, but with the winter mean (DJF) data from 1950 to 1999. The structure of the AO in Fig. 7 is nearly identical to that in Fig. 5. The variance increases from 5.7% for the daily data to 13.9% for the monthly mean data and to 21.0% for the winter mean (DJF) data. EOF-2 explains 10.3% of the total variance of the winter mean data. The structure indicates an NAO-like pattern over the Atlantic sector while the Pacific sector clearly indicates a PNA-like pattern, as discussed by Wallace and Thompson (2002).

The time spectrum of the daily AO index for EOF-1 is plotted in Fig. 8. The result is characterized by a red noise spectrum over the higher frequency range. The red noise turns to white noise for the period longer than 4 months. It is interesting to note that the AO is the most dominant mode from the daily timescale to the decadal timescale, but there is no obvious peak in the time spectrum.

With the same procedure as to obtain the AO in Fig. 5 from the state variable w_i, we can examine the most dominant mode for the external forcing s_i. Figure 9 illustrates the structure of the EOF-1 for the external forcing computed with the daily data. The structure clearly shows the characteristics of synoptic-scale disturbances of zonal wavenumber 6 in the midlatitudes, located along the Pacific storm track. EOF-2 has a similar structure as EOF-1, but with a phase shift by 90° for the zonal wavenumber 6. The combination of these two modes represents the progressive zonal wavenumber 6 along the Pacific storm track. A similar synoptic-scale forcing is seen along the Atlantic storm track in the higher EOF modes. These forcings represent the barotropic–baroclinic interactions g_i in (7) associated with baroclinic instability as parameterized by Tanaka (1998). The storm track analyzed by the transient bar-

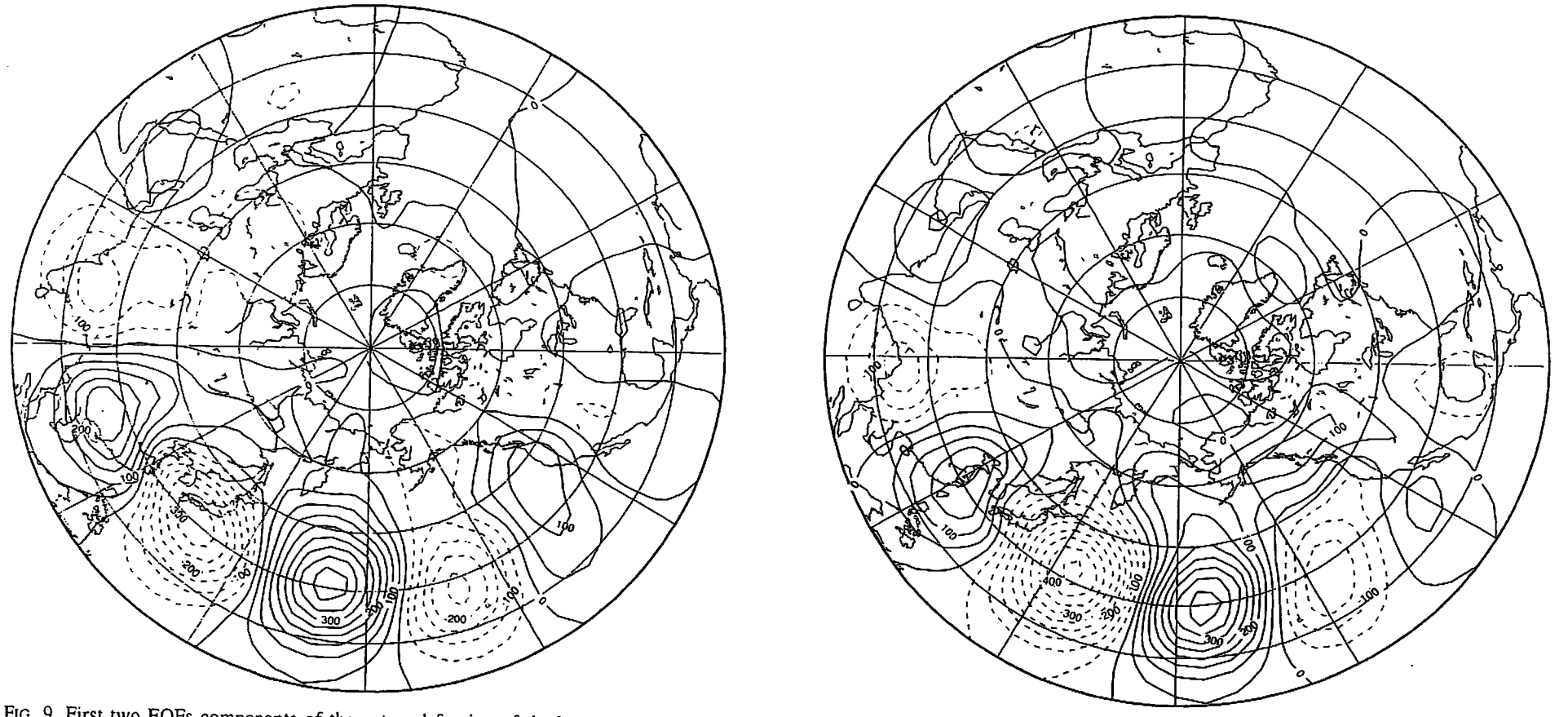

FIG. 9. First two EOFs components of the external forcing of the barotropic component of the atmosphere, analyzed by the forcing s_l with the daily NCEP–NCAR reanalysis from 1950 to 1999.

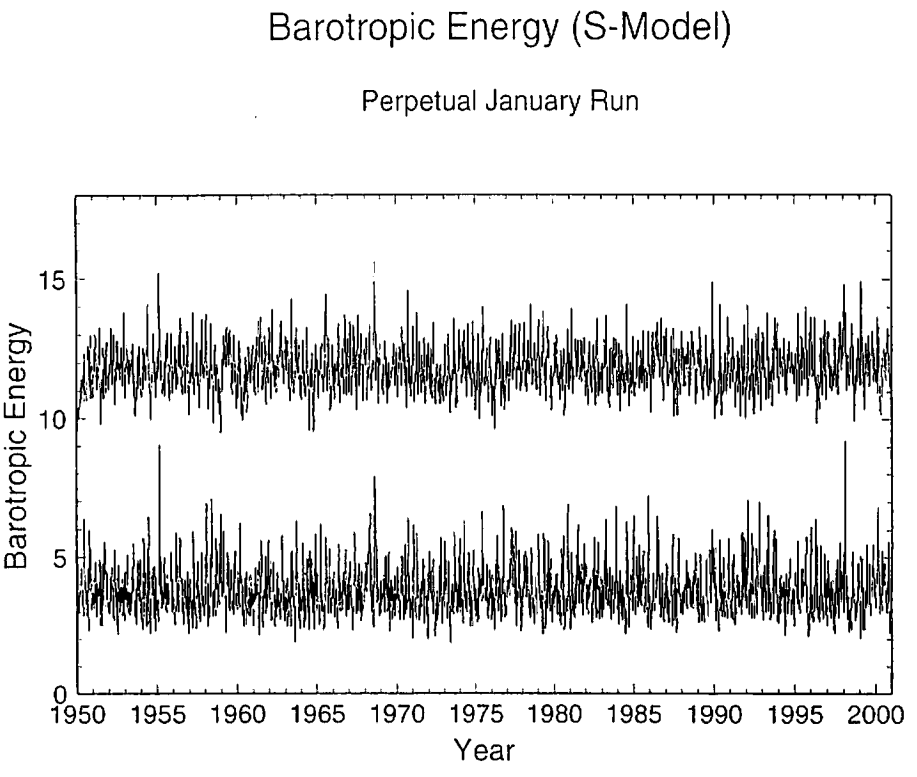

FIG. 10. Daily time series of barotropic energy for the perpetual Jan run of the barotropic S mode for 51 yr. The upper and lower lines represent zonal ($n = 0$) and eddy ($n \neq 0$) energy, respectively. (Unit: 10^5 J m^{-2}.)

otropic height (not shown) is located rather north and downstream of the jet exit region as a response to the baroclinic forcing.

It is important to note that the major energy source of the barotropic component of the atmosphere appears in the synoptic-scale baroclinic eddies. The major response to the forcing, however, appears as the zonally symmetric annular mode. The nonlinear response to the synoptic-scale forcing may be connected by the upscale energy cascade governed by the internal barotropic dynamics.

4. Dominant modes of the model atmosphere

a. Perpetual January run of the barotropic S model

In this section, the barotropic S model of (7) is integrated for 51 yr starting from the initial condition of 0000 UTC 1 January 1950 under the perpetual January condition. The time series of zonal energy ($n = 0$) and eddy energy ($n \neq 0$) are plotted in Fig. 10. Since the initial condition is set on 1 January 1950, the abscissa is numbered, for convenience, from 1950 to 2000. The mean energy levels are approximately 12 and 4×10^5 J m^{-2} for zonal and eddy energies, respectively. Those energy levels are consistent with winter observations in Fig. 4. The energy levels fluctuate with respect to time within 10 to 14×10^5 J m^{-2} for zonal energy and 3 to 6×10^5 J m^{-2} for eddy energy, respectively. No smoothing is applied in this figure. The fluctuation may be regarded totally as the natural variability of the model atmosphere since all model parameters and forcing parameters are fixed.

Figure 11 plots the mean barotropic height for the perpetual January run for 51 yr. There are three major troughs over Japan, the east coast of the United States, and Europe. Although the details are different, to some extent, the overall features of the winter climate in Fig. 1 is simulated. The locations of storm tracks analyzed for the model atmosphere (not shown) agree quite well with observations. Therefore, both mean and transient fields are well described by the barotropic S model.

b. EOF analysis of the model atmosphere

The EOF analysis is conducted for the time series of the model atmosphere with the same method used for the observed atmosphere discussed in section 3. Figure 12 illustrates the first two EOF components of the model atmosphere analyzed by the time series of w_i. For the 50-yr model run with the sample size of $N = 74\,512$, the eigenvalues are well separated according to the significance test by North et al. (1982). The structure of EOF-1 indicates a negative region in high latitudes surrounded by a positive region in the midlatitudes. The positive region shows two peaks over the Pacific and Atlantic sectors. The zero crossing is located around 60°N. The structure is almost identical with the AO analyzed by the observed atmosphere in Fig. 5. Hence, EOF-1 in the model atmosphere may be identified as the AO. The positive peak over the Pacific sector is elongated in the zonal direction, which disagrees to some extent with observation. The elongated positive area in the observed Atlantic sector is now disconnected

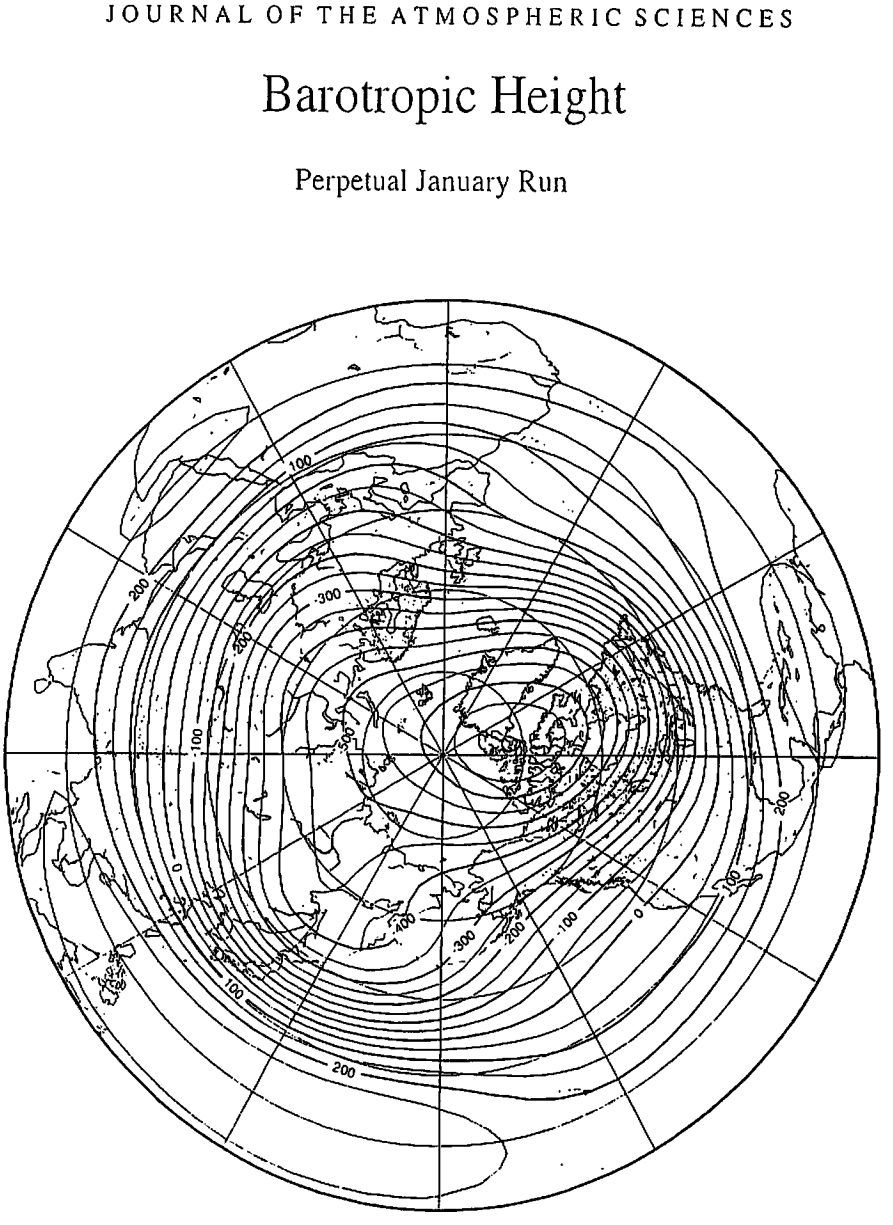

FIG. 11. Mean barotropic height (in m) for the perpetual Jan run for 51 yr.

at the eastern Atlantic in the model. Although there are some differences, the overall features agree quite well with the observation in Fig. 5.

The score time series (365-day running mean) of the EOFs are plotted in Fig. 13. The time series of EOF-1 show a large interannual variability with 2–3-yr periods, similar to the observation in Fig. 6. The decadal variability seems to be absent for the model. EOF-1 explains 15.6% of the total variance of the daily data. The large contribution of the AO may be a result from the relatively weak transient eddies in the synoptic and short waves in the model atmosphere. It is evident from the result that the natural variability associated with the AO can be produced by the internal dynamics of the barotropic atmosphere.

EOF-2 explains 7.9% of the total variance of the daily data. There is a positive peak over the Atlantic sector that extends over North America. The Arctic is negative and the Pacific is also negative. The structure of EOF-2 agrees well with the observed EOF-2 in Fig. 5. The main discrepancy may be seen in the location and strength of the positive peak over Russia. Yet, the overall agreement with observation suggests that the barotropic S model captures not only the essential features of EOF-1 but also that of EOF-2 of the observed atmosphere. The score time series of EOF-2 indicates a larger interannual variability than that of the observation. The dominant periodicity of 2–3 yr agrees with the observation in Fig. 6.

We have compared the structures and the score time series of EOF-3 and EOF-4 with those of the observation (not shown). The result shows not only EOF-1 but also EOF-2 to EOF-4 agree fairly well with the observed EOFs. Therefore, it is confirmed in this study that the major characteristics of the atmospheric low-frequency variability have been captured satisfactorily by the barotropic S model.

The time spectrum of the daily AO index for the model atmosphere is plotted in Fig. 14. The red noise spectrum at the high-frequency range extends up to

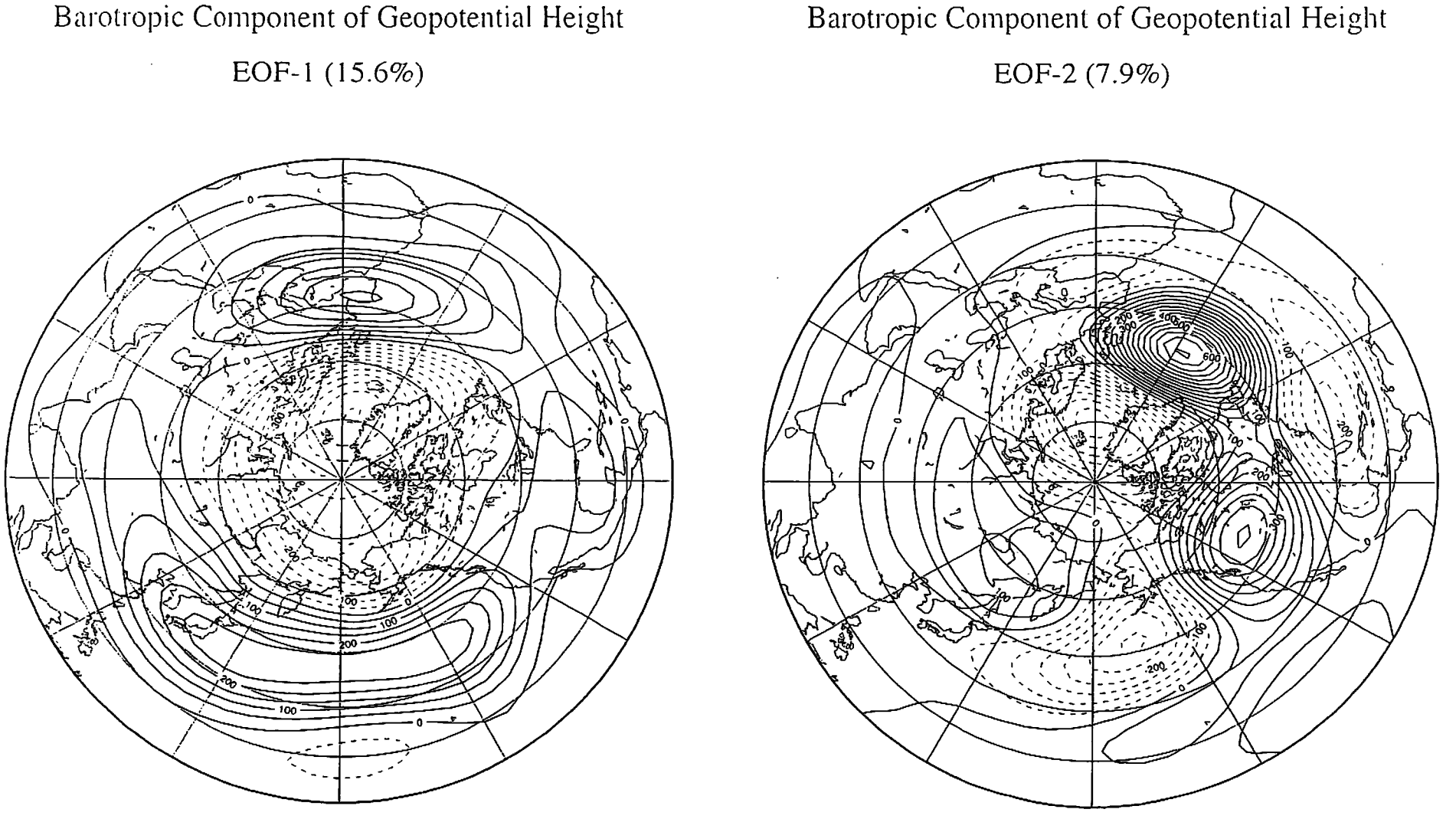

FIG. 12. As in Fig. 5, but for the perpetual Jan run of the barotropic S model for 51 yr.

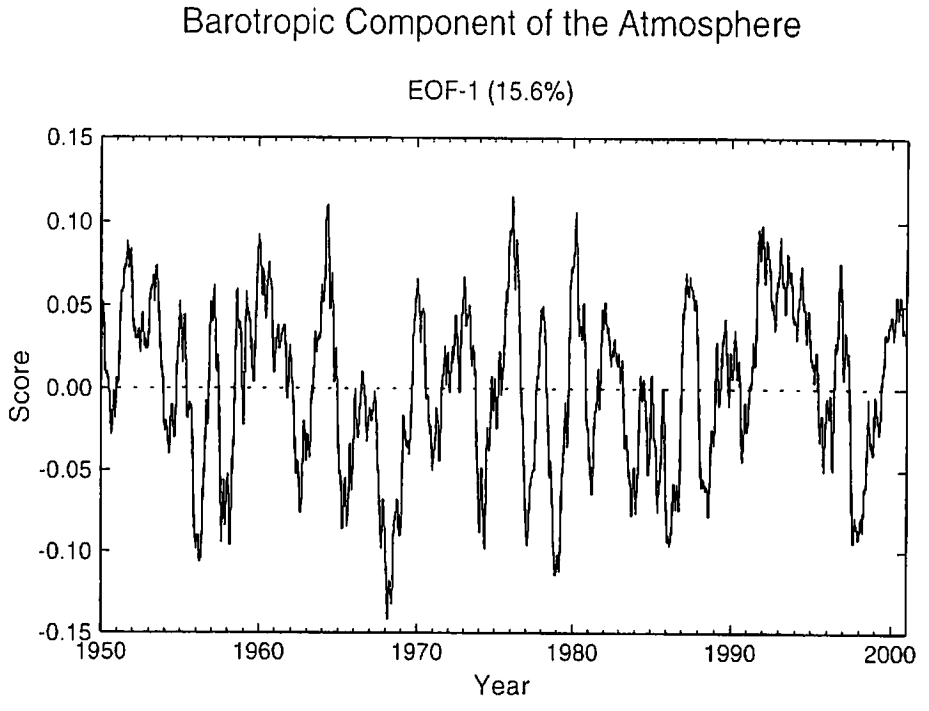

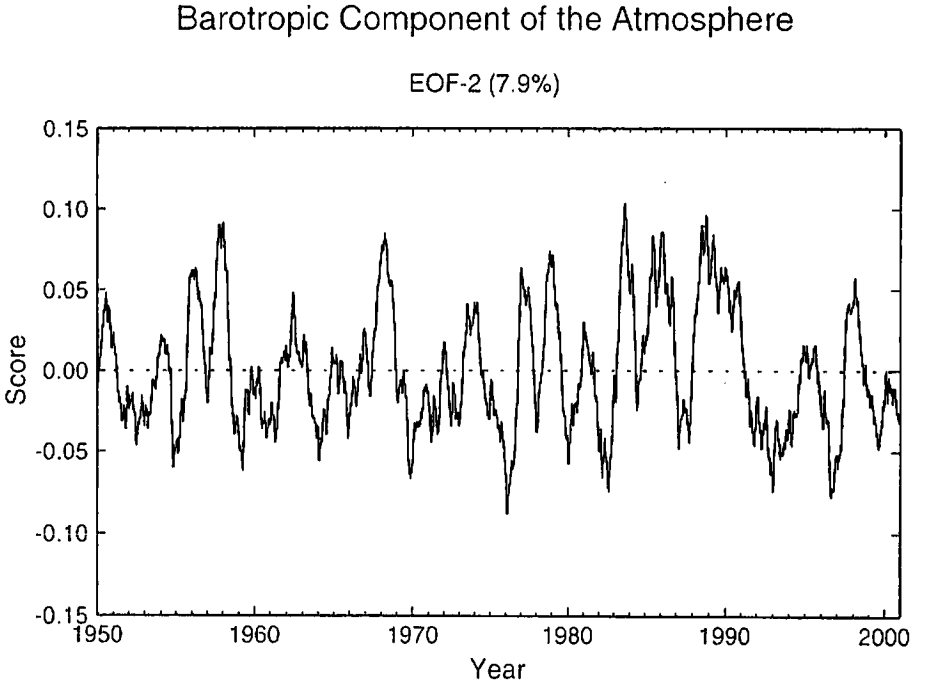

FIG. 13. As in Fig. 6, but for the perpetual Jan run of the barotropic S model for 51 yr.

the period of 4 months, then it shifts to the white noise spectrum at the low-frequency range. There is a minor spectral peak at 2-yr period, and the decadal variability is absent in the result. According to the result of the 500-yr perpetual January run (not shown here), we confirmed that the white noise extends all the way to the low-frequency range. In the observed atmosphere in Fig. 8, the shift from red noise to white noise occurs gradually around the same period. The spectrum is similar to that argued by James and James (1992). Since the white noise is characterized by the variability that has no memory in the past, the clear shift from the red noise to white noise suggests that the barotropic model has a memory up to 4 months as long as the AO index is concerned. The result suggests that the AO index has no specific periodicity, and the variation may be considered as a natural variability of stochastic random noise.

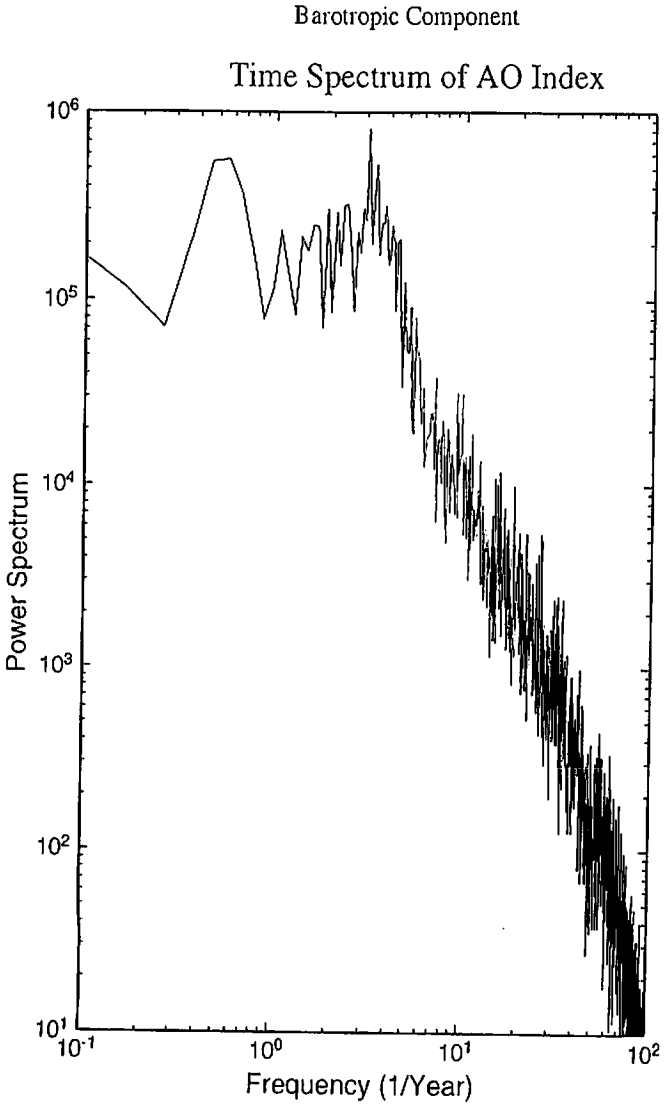

FIG. 14. As in Fig. 8, but for the perpetual Jan run of the barotropic S model for 51 yr.

TABLE 1. Time-mean (1 yr) energy (10^5 J m^{-2}) and energy conversions (10^{-3} W m^{-2}) for the barotropic S model as functions of the zonal wavenumber n. The symbol EN represents total energy, AB system forcing, BC baroclinic instability, NL nonlinear wave–wave interaction, DS surface friction, DF diffusion, and FN total external forcing.

n	EN	AB	BC	NL	DS	DF	FN
0	1 208 261	−114	0	235	−86	−36	−236
1	115 707	16	0	76	−60	−32	−75
2	70 069	169	1	−109	−39	−22	109
3	108 319	141	0	−50	−56	−33	53
4	24 646	30	7	0	−14	−16	8
5	29 521	5	54	−11	−15	−18	25
6	24 069	34	56	−37	−11	−18	62
7	19 117	16	77	−26	−10	−20	64
8	11 316	17	55	−17	−6	−17	49
9	4 794	6	23	0	−2	−10	16
10	2 989	5	12	3	−1	−9	7
11	1 376	2	4	5	−1	−6	0
12	794	0	1	6	0	−4	−3
13	436	1	0	4	0	−3	−2
14	235	0	0	3	0	−2	−2
15	153	0	0	2	0	−2	−1
16	99	1	0	1	0	−1	−1
17	66	0	0	1	0	−1	−1
18	45	0	0	1	0	−1	−1
19	28	0	0	1	0	−1	−1
20	19	0	0	0	0	−1	0

5. Energetics of the model atmosphere

a. Energy spectrum and conversions

In this section, the energy spectrum and conversions of the model atmosphere is compared with observations. Figure 15 plots the barotropic ($m = 0$) energy spectrum of $E_i = E_{nlm}$ as a function of the scale index $|c_i| = |c_{nlm}|$ evaluated for the model atmosphere for 1 yr. In order to avoid the influence of the initial condition, the second year of the time integration was analyzed. The energy distribution compares well with the observations in Fig. 2. The peak of the energy spectrum for the zonal eddy $n \neq 0$ is determined by Rhines' scale, where the inverse energy cascade terminates (Rhines 1979). The spectrum for $n = 0$ coincides with that of $n \neq 0$ for a smaller $|c_i|$, but it continues to increase for larger $|c_i|$. The inverse energy cascade continues to an even larger scale for $n = 0$. The energy level is lower than observations for short waves with smaller $|c_i|$.

The AO or NAM can be characterized by variations in zonally symmetric component of $n = 0$. It is an interesting subject to analyze the energy source and sink for the zonal flows in the model atmosphere. The mean (1 yr) energy levels and energy conversions are computed based on Tanaka (1998), and the result is listed in Table 1 as functions of zonal wavenumber n. Both total energy (EN) and total external forcing (FN) can be assessed directly from the observation. The contributions from the climate forcing $\tilde{s}_i$ are added, for convenience, to the system forcing (AB).

The mean zonal energy is 12.1 × 10^5 J m^{-2}, which is comparable with observations. Two spectral peaks are seen for EN at the wavenumbers $n = 1$ and 3, and the energy level decreases for short waves. The energy levels for short waves are smaller than the observation in Fig. 3 since there is no energy source in this range. The synoptic energy source is transformed mostly to large-scale motions and little comes to short waves under the restriction of the barotropic dynamics.

Here AB excites planetary waves representing the topographic forcing, and a minor energy supply is seen at the synoptic-scale waves. This term works as an energy sink for $n = 0$. The weak energy supply at the synoptic-scale waves is compensated by the baroclinic instability (BC). The nonlinear wave–wave interactions (NL) redistribute the energy from synoptic and planetary waves to mostly zonal motions by the nature of the barotropic dynamics. The wavenumber one and short waves also obtain energy by (NL). The energy is dissipated by the surface friction (DS) and diffusion (DF). The sum of these conversion terms is listed in the total external forcing. The results in this study are quite rea-

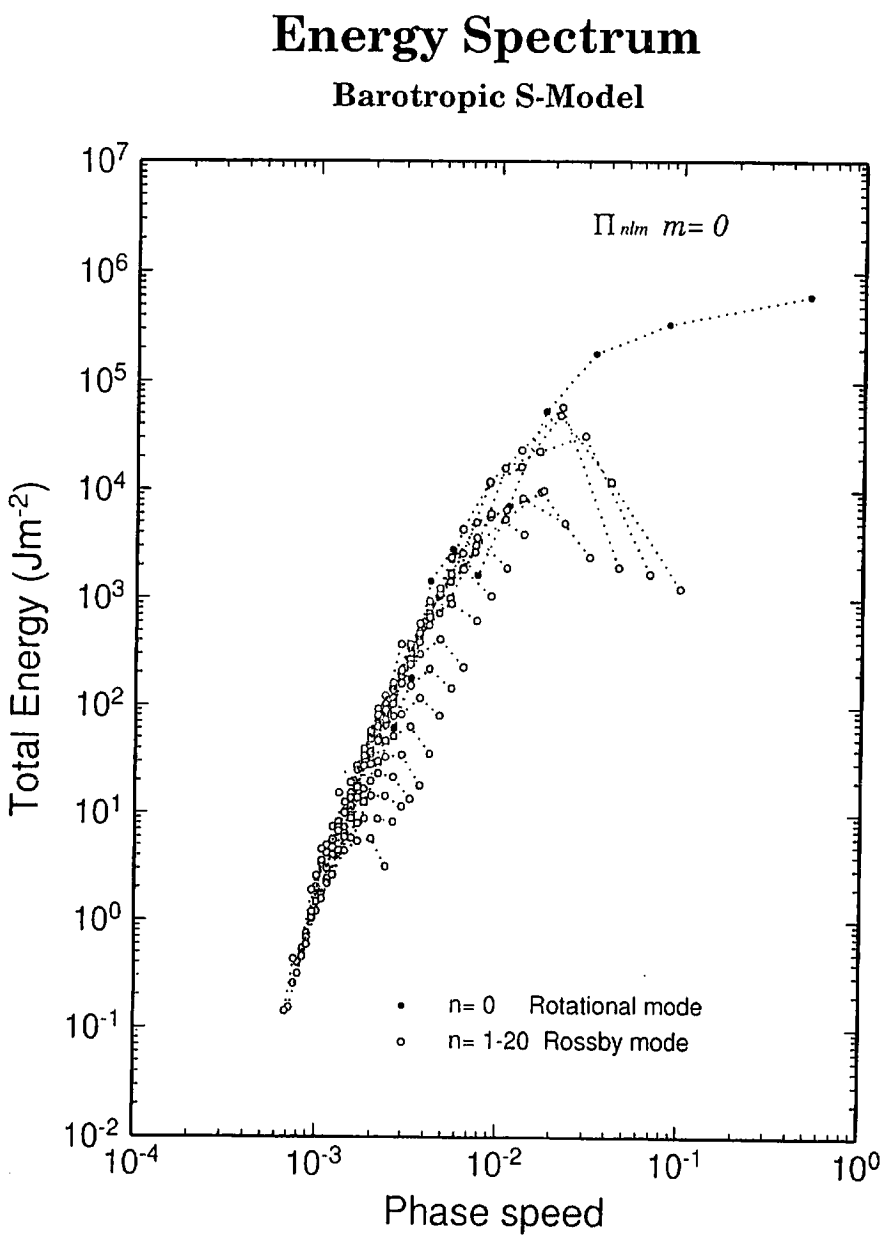

FIG. 15. As in Fig. 2, but for the perpetual Jan run of the barotropic S model for 1 yr. The black and white dots denote $n = 0$ and $n \neq 0$, respectively. (Unit: J m^{-2}.)

sonable compared with observations (Tanaka and Kung 1988; Tanaka 1998).

The result of the energetics analysis indicates two major energy sources at synoptic-scale eddies and planetary waves. The energy is redistributed mostly to zonal motion by the nonlinear upscale energy cascade within a framework of the barotropic dynamics (see Fig. 2). The nonlinear upscale energy cascade by NL is the sole energy supply for the zonal motions where the NAM is contained.

b. *Energetics of the anomaly field*

The AO or NAM can be analyzed as the variation in the anomaly field, especially for the zonally symmetric component of $n = 0$. For this reason, a similar energetics analysis is conducted for the anomaly field of the model atmosphere in this section. The energy spectrum is evaluated for anomaly w_i' and is plotted in Fig. 16 as a function of $|c_i|$. We can notice that the zonal energy (black dots) is reduced substantially compared with that in Fig. 15. The result suggests that the large fraction of zonal energy is contained in steady motions. The spectral peak in the zonal eddy (white dots) is also reduced, indicating that a large fraction of planetary waves are explained by the steady component induced by topographic forcing. However, the energy levels for the synoptic and short waves are comparable with those in Fig. 15, showing the dominant transient motions for these eddies. The energy peak for the anomaly field appears in the intermediate scale of zonal field. The energy peak level for $n = 0$ is as large as that of zonal eddy $n \neq 0$. It is in this range where the characteristics of the AO or NAM are contained.

The mean (1 yr) energy levels and energy conversions for the anomaly field are listed in Table 2 as functions of

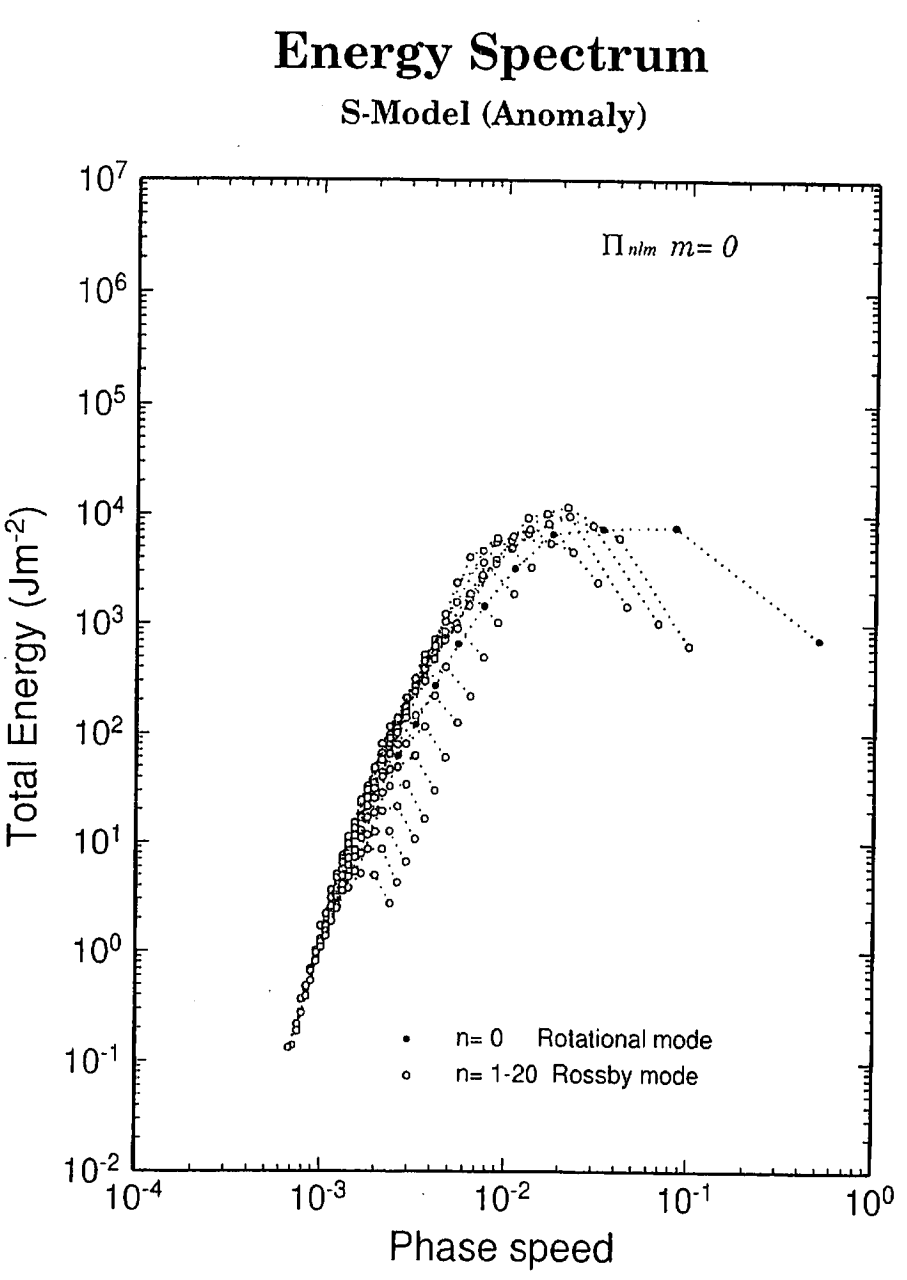

FIG. 16. As in Fig. 15, but for the anomaly of the model atmosphere w_i'. The black and white dots denote $n = 0$ and $n \neq 0$, respectively. (Unit: J m^{-2}.)

zonal wavenumber n. All variables including the nonlinear term are separated in the mean and anomaly, and the energy budget is computed with those anomalies. The EN levels are comparable for $n = 0, \ldots, 5$, and the peak is seen at $n = 1$. The BCs are the main energy source of the anomaly for the synoptic-scale transients. The NL term acts to reduce the anomaly for synoptic eddies. On the contrary, the nonlinear term appears to be the major energy source of the anomaly in planetary waves and the zonal motions. Here DS and DF act to reduce the anomaly for all scale of motions. It is interesting to note that AB is not the energy source but a sink of the anomaly field in planetary waves. The system forcing represents mostly the topographic forcing. The large energy source of AB in Table 1 is thus explained by a steady forcing induced by the topography. This term rather acts to reduce the anomaly in planetary waves.

A large time variation is a notable feature of the NL term. Therefore, a large fraction of the time variation associated with NAM can be explained by the chaotic fluctuation of NL, which is the sole energy source of the transient anomalies in planetary waves and zonal motions.

6. Discussion and conclusions

In this study, a numerical simulation of the Arctic Oscillation (AO) is conducted using a simple barotropic model that considers the barotropic–baroclinic interactions as the external forcing. The model is referred to as a barotropic S model since the external forcing is obtained statistically from the long-term historical data solving an inverse problem. We have integrated the S model for 51 yr under the perpetual January condition

TABLE 2. Time-mean (1 yr) energy (10^5 J m^{-2}) and energy conversions (10^{-3} W m^{-2}) for the anomaly of the S model as functions of the zonal wavenumber n. The symbols are as in Table 1.

n	EN	AB	BC	NL	DS	DF	FN
0	31 639	−17	0	44	−19	−7	−43
1	36 634	−19	0	56	−20	−14	−53
2	31 125	−5	1	37	−17	−13	−34
3	22 917	−3	0	32	−13	−12	−28
4	21 333	5	6	23	−12	−13	−14
5	23 153	8	50	−15	−12	−16	30
6	19 586	15	59	−22	−10	−17	47
7	15 806	21	69	−32	−8	−17	66
8	8 716	14	43	−14	−4	−13	39
9	4 367	5	20	0	−2	−9	13
10	2 380	2	9	5	−1	−7	3
11	1 169	0	3	6	−1	−5	−2
12	633	1	1	4	0	−3	−2
13	362	1	0	3	0	−2	−2
14	198	0	0	2	0	−2	−2
15	118	0	0	2	0	−1	−1
16	78	0	0	1	0	−1	−1
17	47	0	0	1	0	−1	−1
18	33	0	0	1	0	−1	−1
19	21	0	0	1	0	0	0
20	14	0	0	0	0	0	0

and analyzed the dominant EOF modes in the model. The model results are compared with the EOF analysis of the barotropic component of the real atmosphere based on the daily NCEP–NCAR reanalysis for 50 yr from 1950 to 1999.

According to the result, the first EOF of the model atmosphere appears to be the AO similar to the observation. The annular structure of the AO and two centers of action at Pacific and Atlantic sectors are simulated nicely by the barotropic S model. The result suggests that the AO may be understood as the natural variability of the barotropic component of the atmosphere induced by the inherent barotropic dynamics, which is forced by the barotropic–baroclinic interactions. The EOF analysis of the model atmosphere shows not only that EOF-1 but also EOF-2 to EOF-4 agree fairly well with the observed EOFs. Therefore, the characteristics of the atmospheric low-frequency variability have been captured satisfactorily by the barotropic S model.

The EOF analysis is further applied for the external forcing of the barotropic component of the observed atmosphere. According to the result, the most dominant mode of the forcing is the barotropic–baroclinic interactions associated with baroclinic eddies of zonal wavenumber 6 located along the Pacific storm track. A similar synoptic-scale forcing is seen along the Atlantic storm track in the higher EOF modes. The energy source at the synoptic-scale eddies is transformed to zonally symmetric motions by the nonlinear upscale energy cascade, which is the sole energy source of the zonal wavenumber $n = 0$. Hence, the annular structure of the AO or NAM has been excited by the nonlinear upscale energy cascade from active transient eddies along the storm tracks. The positive feedback between transient eddies and zonal motions can be one of the possible excitation mechanism of the AO (Lorenz and Hartmann 2001; Tanaka and Tokinaga 2002).

There are two active storm tracks over the Pacific and Atlantic sectors. These two storm tracks are known to behave independently, indicating insignificant correlation with each other (Ambaum et al. 2001). When the Atlantic storm track produces positive and negative height anomalies over the Atlantic and the Arctic, respectively, the annular structure appears excited by the energy supply to the zonal motion. Similarly, when the Pacific storm track produces positive and negative height anomalies over the Pacific and the Arctic, respectively, the same annular structure appears excited by the energy supply to the zonal motion. Although the activities of the two storm tracks are independent and not correlated with each other, the statistical EOF analysis reveals a single negative height anomaly over the Arctic and two positive height anomalies over the Pacific and Atlantic sectors, as demonstrated by Deser (2000), Ambaum et al. (2001), and Wallace and Thompson (2002). EOF-2 indicates opposite signs over the Pacific and Atlantic sectors in order to describe the independent behavior between the two sectors as demonstrated in this study with the barotropic S model.

The zonally symmetric annular mode would be excited when the storm track is distributed uniformly as seen in the SAM. In the Northern Hemisphere, the AO or NAM would be excited both by transient synoptic eddies along the storm tracks and standing planetary waves. The upscale energy cascade from those eddies or waves to zonal motions would produce the largest-scale annular mode of $n = 0$, which can exist in both hemispheres. The zonally symmetric annular mode can be excited by various arbitrary forcing such as a volcanic effect, global warming, or the Milankovitch cycle because the energy of the impact is transformed eventually to the zonal flow by the characteristics of barotropic dynamics. In conclusion, the AO can be dynamically understood as the internal mode of the barotropic atmosphere where the largest-scale annular mode is excited by the nonlinear upscale energy cascade from various energy sources.

Acknowledgments. This research was supported by the IARC/FRSGC. The author appreciates Dr. Taroh Matsuno and Dr. Moto Ikeda for their financial support and Dr. M. Wallace, Dr. D. Thompson, Dr. D. Hartmann, Dr. D. Lorenz, Dr. K. Yamazaki, and Dr. H. Itoh for their meaningful suggestions and discussion. The author appreciate Ms. K. Honda and Mr. D. Nohara for their technical assistance.

REFERENCES

Akahori, K., and S. Yoden, 1997: Zonal flow vacillation and bimodality of baroclinic eddy life cycles in a simple global circulation model. *J. Atmos. Sci.*, **54**, 2349–2361.

Ambaum, M. H. P., B. J. Hoskins, and D. B. Stephenson, 2001: Arctic oscillation or North Atlantic oscillation? *J. Climate,* **14,** 3495–3507.

Boer, G. J., S. Fourest, and B. Yu, 2001: The signature of the annular modes in the moisture budget. *J. Climate,* **14,** 3655–3665.

Deser, C., 2000: On the teleconnectivity of the Arctic oscillation. *Geophys. Res. Lett.,* **27,** 779–782.

Feldstein, S. B., 2002: The recent trend and variance increase of the annular mode. *J. Climate,* **15,** 88–94.

——, and S. Lee, 1998: Is the atmospheric zonal index driven by an eddy feedback? *J. Atmos. Sci.,* **55,** 3077–3086.

Fyfe, J. C., G. J. Boer, and G. M. Flato, 1999: The Arctic and Antarctic oscillations and their projected changes under global warming. *Geophys. Res. Lett.,* **26,** 1601–1604.

Hartmann, D. L., 1995: A PV view of zonal flow vacillation. *J. Atmos. Sci.,* **52,** 2561–2676.

——, and F. Lo, 1998: Wave-driven zonal flow vacillation in the Southern Hemisphere. *J. Atmos. Sci.,* **55,** 1303–1315.

James, I. N., and P. M. James, 1992: Spatial structure of ultra-low frequency variability of the flow in a simple atmospheric circulation model. *Quart. J. Roy. Meteor. Soc.,* **118,** 1211–1233.

Kalnay, E. M., and Coauthors, 1996: The NCEP/NCAR 40-year Reanalysis Project. *Bull. Amer. Meteor. Soc.,* **77,** 437–471.

Karoly, D. J., 1990: The role of transient eddies in the low-frequency zonal variations in the Southern Hemisphere circulation. *Tellus,* **42A,** 41–50.

Kasahara, A., 1976: Normal modes of ultralong waves in the atmosphere. *Mon. Wea. Rev.,* **104,** 669–690.

——, 1977: Numerical integration of the global barotropic primitive equations with Hough harmonic expansions. *J. Atmos. Sci.,* **34,** 687–701.

——, 1978: Further studies on a spectral model of the global barotropic primitive equations with Hough harmonic expansions. *J. Atmos. Sci.,* **35,** 2043–2051.

Kidson, J. W., and M. R. Sinclair, 1995: The influence of persistent anomalies on Southern Hemisphere storm tracks. *J. Climate,* **8,** 1938–1950.

Kitoh, A., H. Koide, K. Kodera, S. Yukimoto, and A. Noda, 1996: Interannual variability in the stratospheric–tropospheric circulation in a coupled ocean–atmosphere GCM. *Geophys. Res. Lett.,* **23,** 543–546.

Kodera, K., M. Chiba, H. Koide, A. Kitoh, and Y. Nikaidou, 1996: Interannual variability of winter stratosphere and troposphere in the Northern Hemisphere. *J. Meteor. Soc. Japan,* **74,** 365–382.

Lee, S., and S. B. Feldstein, 1996: Mechanism of zonal index evolution in a two-layer model. *J. Atmos. Sci.,* **53,** 2232–2246.

Limpasuvan, V., and D. L. Hartmann, 1999: Eddies and the annular modes of climate variability. *Geophys. Res. Lett.,* **26,** 3133–3136.

——, and ——, 2000: Wave-maintained annular modes of climate variability. *J. Climate,* **13,** 4144–4429.

Lorenz, D. J., and D. L. Hartmann, 2001: Eddy–zonal flow feedback in the Southern Hemisphere. *J. Atmos. Sci.,* **58,** 3312–3327.

North, G. R., T. L. Bell, and R. F. Cahalan, 1982: Sampling errors in the estimation of empirical orthogonal functions. *Mon. Wea. Rev.,* **110,** 699–706.

Rhines, P. B., 1979: Geostrophic turbulence. *Annu. Rev. Fluid Mech.,* **11,** 401–441.

Robertson, A. W., 2001: Influence of ocean–atmosphere interaction on the Arctic oscillation in two general circulation models. *J. Climate,* **14,** 3240–3254.

Robinson, W. A., 1991: The dynamics of the zonal index in a simple model of the atmosphere. *Tellus,* **43A,** 295–305.

——, 1994: Eddy feedbacks on the zonal index and eddy–zonal flow interactions induced by zonal flow transience. *J. Atmos. Sci.,* **51,** 2553–2562.

——, 1996: Does eddy feedback sustain variability in the zonal index? *J. Atmos. Sci.,* **53,** 3556–3569.

Shigehisa, Y., 1983: Normal modes of the shallow water equations for zonal wavenumber zero. *J. Meteor. Soc. Japan,* **61,** 479–494.

Shindell, D. T., R. L. Miller, G. A. Schmidt, and L. Pandolfo, 1999: Simulation of recent northern winter climate trends by greenhouse-gas forcing. *Nature,* **399,** 452–455.

Shiotani, M., 1990: Low-frequency variations of the zonal mean state of the Southern Hemisphere troposphere. *J. Meteor. Soc. Japan,* **68,** 461–471.

Tanaka, H. L., 1985: Global energetics analysis by expansion into three dimensional normal mode functions during the FGGE winter. *J. Meteor. Soc. Japan,* **63,** 180–200.

——, 1991: A numerical simulation of amplification of low-frequency planetary waves and blocking formations by the up-scale energy cascade. *Mon. Wea. Rev.,* **119,** 2919–2935.

——, 1998: Numerical simulation of a life-cycle of atmospheric blocking and the analysis of potential vorticity using a simple barotropic model. *J. Meteor. Soc. Japan,* **76,** 983–1008.

——, and E. C. Kung, 1988: Normal mode energetics of the general circulation during the FGGE year. *J. Atmos. Sci.,* **45,** 3723–3736.

——, and ——, 1989: A study of low-frequency unstable planetary waves in realistic zonal and zonally varying basic states. *Tellus,* **41A,** 179–199.

——, and S. Sun, 1990: A study of baroclinic energy sources for large-scale atmospheric normal modes. *J. Atmos. Sci.,* **47,** 2674–2695.

——, and A. Kasahara, 1992: On the normal modes of Laplace's tidal equations for zonal wavenumber zero. *Tellus,* **44A,** 18–32.

——, and D. Nohara, 2001: A study of deterministic predictability for the barotropic component of the atmosphere. Science Rep. 22A, Institute Geoscience, University of Tsukuba, 45 pp.

——, and H. Tokinaga, 2002: Baroclinic instability in high latitudes induced by polar vortex: A connection to the Arctic oscillation. *J. Atmos. Sci.,* **59,** 69–82.

Thompson, D. W. J., and J. M. Wallace, 1998: The Arctic oscillation signature in the wintertime geopotential height and temperature fields. *Geophys. Res. Lett.,* **25,** 1297–1300.

——, and ——, 2000: Annular modes in the extratropical circulation. Part I: Month-to-month variability. *J. Climate,* **13,** 1000–1016.

Wallace, J. M., 2000: North Atlantic oscillation/annular mode: Two paradigms—One phenomenon. *Quart. J. Roy. Meteor. Soc.,* **126,** 791–805.

——, and D. W. J. Thompson, 2002: The Pacific center of action of the Northern Hemisphere annular mode: Real or artifact? *J. Climate,* **15,** 1987–1991.

Winkler, C. R., M. Newman, and P. D. Sardeshmukh, 2001: A linear model of wintertime low-frequency variability. Part I: Formulation and forecast skill. *J. Climate,* **14,** 4474–4494.

Yamazaki, K., and Y. Shinya, 1999: Analysis of the Arctic oscillation simulated by AGCM. *J. Meteor. Soc. Japan,* **77,** 1287–1298.

Yu, J. Y., and D. L. Hartmann, 1993: Zonal flow vacillation and eddy forcing in a simple GCM of the atmosphere. *J. Atmos. Sci.,* **50,** 3244–3259.